EXPERIMENTAL CHARACTERIZATION OF STROKE FAILURE OF HARD DISK DRIVE WITH NANOPOSITIONING PZT

HUSSADIN THUNGSAKUL

A THESIS SUBMITTED IN PARTIAL FULFILLMENT

OF THE REQUIREMENT FOR THE DEGREE OF

MASTER OF ENGINEERING IN DATA STORAGE TECHNOLOGY

ENGLISH PROGRAM

INTERNATIONAL COLLEGE

KING MONGKUT'S INSTITUTE OF TECHNOLOGY LADKRABANG

2013

KMITL-2013-IC-M-005-0011

หัวข้อวิทยานิพนธ์	การวิเคราะห์เชิงทดลองของการเกิดความเสียหายสโตรคของฮาร์ดดิสก์ไดร์ฟที่ประกอบด้วยพีแซดทีเคลื่อนที่ระดับนาโนเมตร
นักศึกษา	นายหัสดินทร์ ตั้งสกุล
รหัสประจำตัว	52600613
ปริญญา	วิศวกรรมศาสตร์มหาบัณฑิต
ภาควิชา	เทคโนโลยีการบันทึกข้อมูล
พ.ศ.	2556
อาจารย์ที่ปรึกษาวิทยานิพนธ์	ดร. วินัดดา วงศ์วิริยะพันธ์
อาจารย์ที่ปรึกษาวิทยานิพนธ์ร่วม	รศ. ดร. วันชัย ไพจิตโรจนา

บทคัดย่อ

งานวิจัยนี้ได้ทำการวิเคราะห์เชิงทดลองของการเกิดความเสียหายสโตรคของฮาร์ดดิสก์ไดร์ฟที่ประกอบด้วยพีแซดทีเคลื่อนที่ระดับนาโนเมตร ได้แบ่งงานวิจัยเป็นสี่ส่วน ในส่วนแรกได้ศึกษาผลกระทบเชิงกลที่มีผลทำให้สมบัติของพีแซดทีด้อยลง โดยวิเคราะห์สัณฐานวิทยาด้วยเครื่องเอ็กซ์เรย์และกล้องจุลทรรศน์อิเล็กตรอนแบบส่องกราด และตรวจสอบรอยเชื่อมต่อวงจรระหว่างพีแซดทีกับแต่ละจุดเชื่อมต่อวงจร ซึ่งพบว่าลักษณะสัณฐานวิทยาของชิ้นงานดีและชิ้นงานเสียหายไม่มีความแตกต่าง ไม่มีผลกระทบเชิงกลที่ทำให้ชิ้นงานเสียหายทุกจุดที่เชื่อมต่อวงจร ทุกจุดที่เชื่อมต่อกันระหว่างพีแซดทีกับจุดเชื่อมต่อยังมีโครงสร้างและรอยเชื่อมต่อที่ดี ไม่มีผลกระทบเชิงกลที่ทำให้ชิ้นงานเสียหาย ในส่วนที่สองได้ศึกษาสาเหตุของความเสียหายสโตรคในแต่ละขั้นตอนของกระบวนการผลิตเฮทจีเอ (HGA) โดยใช้มัลติมิเตอร์ในการวัดค่า

ประจุไฟฟ้าและความต้านทานไฟฟ้าของพีแซดที พบว่าที่ตู้อบด้วยแสงอินฟาเรดเป็นต้นตอของสาเหตุของค่าประจุไฟฟ้าตกลงไปถึงร้อยละ 30 ในงานวิจัยส่วนที่สามได้ศึกษาสาเหตุที่มีผลกระทบต่อความเสียหายสโตรคในกระบวนการผลิตที่ใช้ตู้อบด้วยแสงอินฟาเรด โดยการปรับระดับพลังงานของแหล่งกำเนิดอินฟาเรดในตู้อบตั้งแต่ 1.5, 2.5, 3.6 และ 4.3 J/cm^2 โดยระดับพลังงานปัจจุบันคือ 3.1 J/cm^{2}หลังจากนั้นทำการวัดค่าประจุไฟฟ้าบนชิ้นงาน พบว่าเมื่อระดับพลังงานอินฟาเรดเท่ากับ 3.1 จูลต่อตารางเซนติเมตร (J/cm^2) ค่าประจุไฟฟ้าที่วัดได้ในแต่ละขั้นตอนของกระบวนการผลิต HGA ยังอยู่ในระดับปลอดภัย เมื่อเพิ่มระดับพลังงานแหล่งจ่ายอินฟาเรดตั้งแต่ 3.1 ถึง 3.3 J/cm^2 เริ่มทำให้มีความเสี่ยงที่จะทำให้เกิดความเสียหายสโตรค และเมื่อเพิ่มระดับพลังงานแหล่งจ่ายอินฟาเรดมากกว่า 3.3 J/cm^2 พบว่าพีแซดทีมีสมบัติเสื่อมถอยลงไปหรือไม่สามารถทำงานได้ เนื่องมาจากความร้อนถ่ายเทจากแสงอินฟาเรดสู่ชิ้นงาน เมื่ออุณหภูมินั้นสูงมากกว่าครึ่งหนึ่งของอุณหภูมิคิวรี่ พีแซดทีจะเริ่มเสื่อมสภาพ และมีสมบัติที่ด้อยลงไป การทดลองสุดท้าย ได้ตรวจสอบสมบัติทางไฟฟ้าของชิ้นงานที่เกิดความเสียหายสโตรค และนำชิ้นงานนั้นมารีโพลิ่งโดยจ่ายค่าความต่างศักย์ 92.5 โวลต์ให้แก่พีแซดทีที่หัวอ่าน เพื่อให้สมบัติทิศทางการเรียงตัวของพีแซดทีไดโพลกลับมาเหมือนเดิม พบว่าหลังจากทำการรีโพลิ่งแล้วค่าประจุไฟฟ้าอยู่ในช่วง 377 ถึง 381 พิโกฟารัดซึ่งเป็นค่าที่อยู่ในช่วงที่ยอมรับได้ นอกจากนี้เมื่อตรวจสอบภาพตัดขวางของชิ้นงานโดยกล้องจุลทรรศน์อิเล็กตรอนแบบส่องกราด พบว่าไม่มีความแตกต่างกันระหว่างชิ้นงานดีและชิ้นงานที่ผ่านการรีโพลิ่ง

Thesis	Experimental Characterization of Stroke Failure of Hard Disk Drive with Nanopositioning PZT
Student	Mr. Hussadin Thungsakul
Student ID.	52600613
Degree	Master of Engineering
Program	Data Storage Technology
Year	2013
Thesis Advisor	Dr. Winadda Wongwiriyapan
Co-Advisor	Assoc. Prof. Dr. Wanchai Pijitrojana

ABSTRACT

This thesis investigated the stroke failure of PZT suspension design. There are four main experiments. The first experiment is to verify mechanical damage or source of PZT degraded by using X-Ray microscope, scanning electron microscope (SEM) for external visual inspection and using shear test to verify the PZT bonding condition and circuit connection to each other. There are no differences in SEM images between good parts and the stroke failure parts. No mechanical damages found at all joint areas and also surfaces of both sides of PZT are in good condition. Moreover after shear test at bonded area, there are no any abnormal structures. The second experiment is to study the source of stressor in HGA manufacturing process by using multi meter to measure capacitance and resistance. It was found that an infrared (IR)

oven is the cause of capacitance increase up to 30%. The third experiment is to study the source of stressor inside the IR Oven cure station by varying an infrared energy level at 1.5, 2.5, 3.6 and 4.3 J/cm^2, while the current energy level in process is at 3.1 J/cm^2. Capacitance was measured after IR oven process. It was found that the energy level less than 3.1 J/cm^2 is no risk and the IR energy level from 3.1 to 3.3 J/cm^2 is risk for stroke failure. Moreover, if the IR energy level is more than 3.3 J/cm^2, PZT is dead. The PZT on suspension degraded or dead due to heat transferred from IR Oven to the parts. Once the temperature increases higher than half of Curie's temperature, PZT material starts to degrade. The last experiment is to verify electrical performance of stroke failure parts after re-poling. Re-poling is the process to restore the piezoelectric properties to the original dipoles orientation by applying voltage of 92.5 V. After re-poling, the capacitance and the normalized stroke are back to normal values within an acceptable operating range (377 to 381 pF). The cross-sectional SEM images show no difference between good parts and stroke failure parts after re-poling.

Acknowledgement

First of all, I would like to thank you Dr. Winadda Wongwiriyapan and Dr. Wanchai Pijitrojana, my Advisor and Co-Advisor respectively for their very helpful recommendation and suggestions with a constant supports of my research at KMITL. I am also thank you to all Thesis committee members for their constructive comments and helpful discussion which guide me a better understanding and perspective on my own result. I also should mention that my graduate study in King Monkut's Instisute of Technology Ladkrabang was supported by NSTDA, KMITL and Seagate Technology (Thailand) Ltd.

And Finally, I would like to acknowledge the support of my family and friends for all of their help.

Hussadin Thungsakul

Bangkok, Thailand

Table of Contents

Acronyms, Definitions and Symbols

This thesis document uses the following set of Acronyms, definitions and symbols

VCM	Voice Coil Motor
AD	Areal Density
PZT	Property of lead Zirconate Titanate
HDD	Hard Disk Drive
DC	Direct Current
EACL	Enhanced Active Constrained Layer
ACL	Active Constrained Layer
PA	Purely Active
PES	Positioning Error System
HGA	Head Gimbal Assembly
TGA	Trace Gimbal Assembly
TIC	Thermal Inter Connect
FOLA	Front of the Line Automation
BOLA	Back of the Line Automation
RFID	Radio Frequency Identification
IR Oven	Infrared Radiation Oven
RSA	Roll Static Adjust
PSA	Pitch Static Adjust
ABS	Air Bearing Surface
HSA	Head Stack Assembly

DNA Deoxyribonucleic Acid

List of Figures

Figure **Page**

List of Figures (Cont.)

Figure **Page**

List of Figures (Cont.)

Figure **Page**

List of Tables

Table **Page**

CHAPTER 1

Introduction

1.1 Problem Statement

High Areal Density (AD) growth rate per Moore's Law from 10% to 30% for Hard Disk Drive Technology. An ultra high precision nano scale for head sensor and media track are required to get more accurate data in hard disk drive manufacturing process. So, the new suspension design with microactuator has been evaluated and assembled in Seagate Thailand and found 100% stroke failures at electrical Tester. This design can not launch for Seagate product due to this problem.

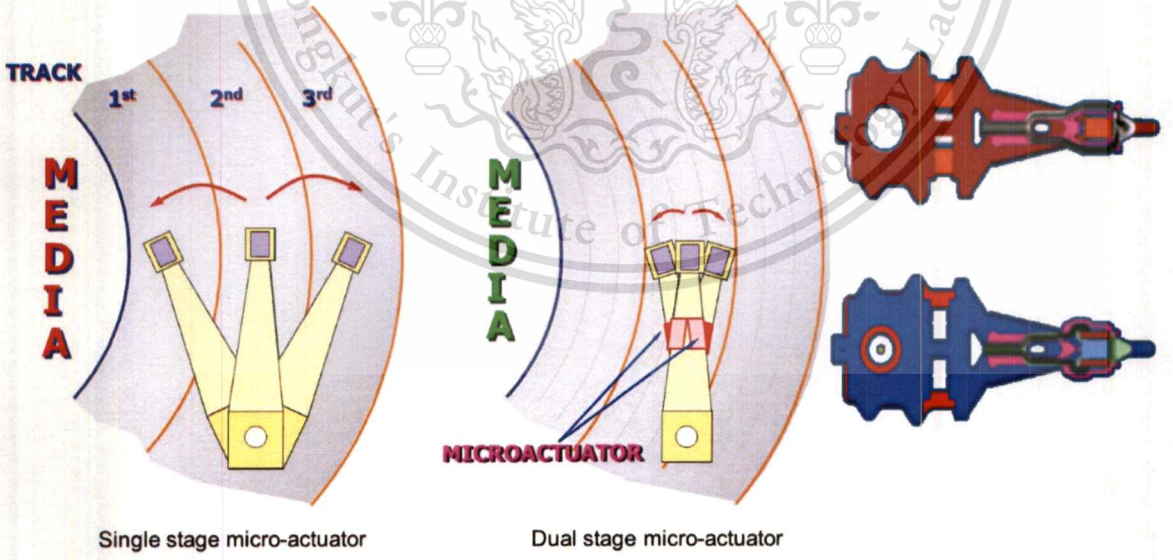

Figure 1.1 High Areal Density Media and Suspension

The main purpose of this thesis is to study and understand piezoelectric theory, failure analysis to identify what kind of stressor is the cause of problem and fix it on time. Seagate new suspension design able to launch the new product and hard disk drive ahead of our competitor.

1.2 Project Objectives

- To study and understand piezoelectricity theory and structure.
- To perform failure analysis to identify the root cause of stroke failure.
- To setup experiment for measuring the stroke at various process steps and comparison to electrical failure.
- To experimentally characterize to get the maximize of head performance.

1.3 Project Goal

To perform failure analysis and experimental characterization to find out the root cause of high stroke failure for the new suspension design.

1.4 Scope of Research

This research will study and understand piezoelectric theory and structure. To investigate and analyze what is the cause of stroke failure

for this new suspension design. Once this problem is fixed, Seagate be able to launch this design on time and ahead of our competitor with higher AD production design.

1.5 Research Metrology

The research merology steps are consist of :-

- Study and understand piezoelectric theory and structure.
- Study and perform failure analysis on stroke failure parts and identify what kind of stressor can cause this failure mode.
- Study theory and relevant parameter of electrical Tester and other characterization tool to verify and analyze the cause of problem.
- Apply stressor simulation to identify the cause of problem
- Conclusions and recommendations

1.6 Literature Review

To obtain more understanding of the related topic and knowledge prior to perform this research, there are six papers for this study. These papers are as follows

1. Piezoelectric ceramic [1]
2. Manufacturing Process of Piezoelectric Thin-Film Dual-Stage Actuator and Its Reliability for HDD [2]
3. Spinstand Control Characterization of an electromagnetic Slider Microactuator [3]

4. Precision Positioning of Hard Disk Drives Using Piezoelectric Actuators with Passive Damping [4]
5. A dual-stage magnetic disk drive actuator using a piezoelectric device for a high track density [5]

[1] B.Jaffe, W.R. Cook and H. Jaffe, "Piezoelectric ceramics", (Academic Press, New York, 1971)

This academic press is provided more details of piezoelectric ceramic theory, material, structure, fabrication and poling piezoelectric. Discovery of piezoelectric effect by Currie brothers (Pierre and Jacques) was done in 1880. The main breakthrough in the field came during early to mid 1940's, with the development of ABO_3 type perovskite structure. Lead zirconate titanate(1-x)PbZrO3 xPbTiO3(PZT) is the most important piezoelectric material which was developed in 1950's, and after 50 years it remains the most widely used piezoelectric ceramic. Large piezoelectric coefficient, large coupling factor and high Curie temperature (T_C) makes this material suitable for a wide range of piezoelectric applications. The piezoelectric includes two type of responses; direct and converse. Production of electric charge when stress is applied is known as direct piezoelectric effect whereas the production of stress and/or strain when an electric field is applied is known as converse piezoelectric effect. The PZT on suspension is converse piezoelectric effect.

Piezoelectric ceramic materials, as stated earlier, are not piezoelectric until the random ferroelectric domains are aligned. This alignment is accomplished through a process known as "poling". Poling consists of inducing a D.C. voltage across the material. The ferroelectric domains align to the induced field resulting in a net piezoelectric effect. It should be noted that not all the domains become exactly aligned. Some of the domains only partially align and some do not align at all. The number of domains that align depends upon the poling voltage, temperature, and the time the voltage is held on the material. During poling the material permanently increases in dimension between the poling electrodes and decreases in dimensions parallel to the electrodes. The material can be depoled by reversing the poling voltage, increasing the temperature beyond the materials Currie point, or by inducing a large mechanical stress.

[2] Hideki Kuwajima, Hirokazu Uchiyama, Yuko Ogawa, Hiroyuki Kita, and Kaoru Matsuoka, "Manufacturing Process of Piezoelectric Thin-Flim Dual-Stage Actuator and Its Reliability for HDD", IEEE Transactions on Magnetics, Vol. 38, No 5, September 2002

This paper is explained about microactuator structure, fabrication and characterization, featuring large displacement of 1.2μm and high-resonance frequency over 15kHz. The reliability against temperature, humidity and mechanical shock were investigated to ensure the practical application to the drive products as shown in Fig. 1.2 -1.4.

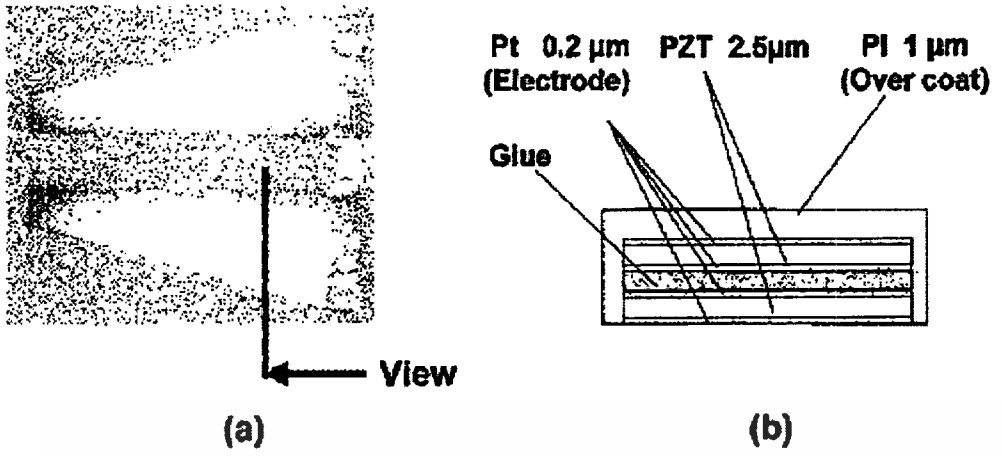

Figure 1.2 The thin-film PZT microactuator element

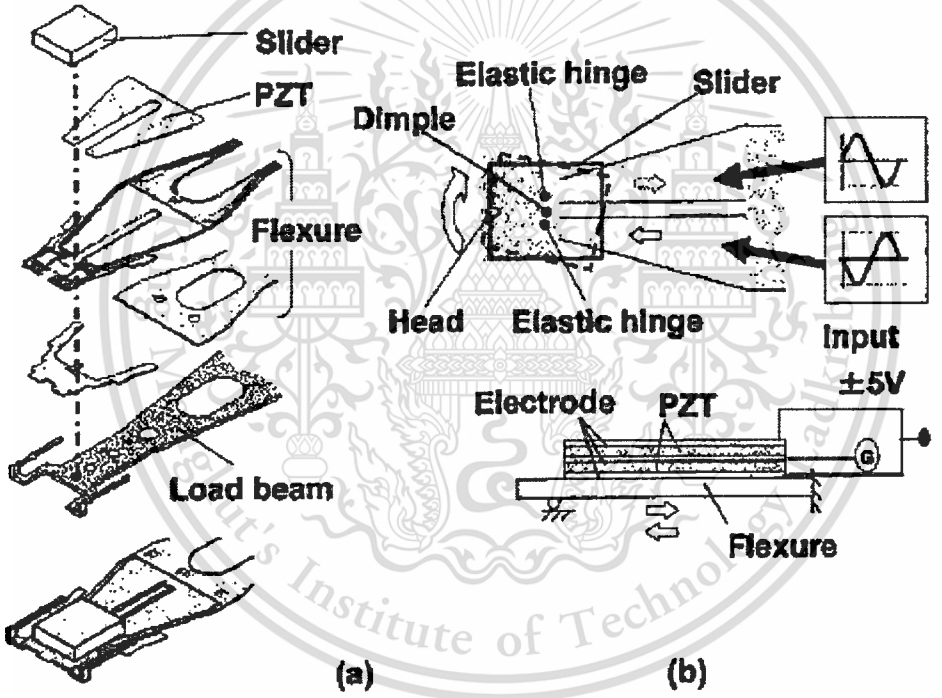

Figure 1.3 Suspension Structure and action of PZT

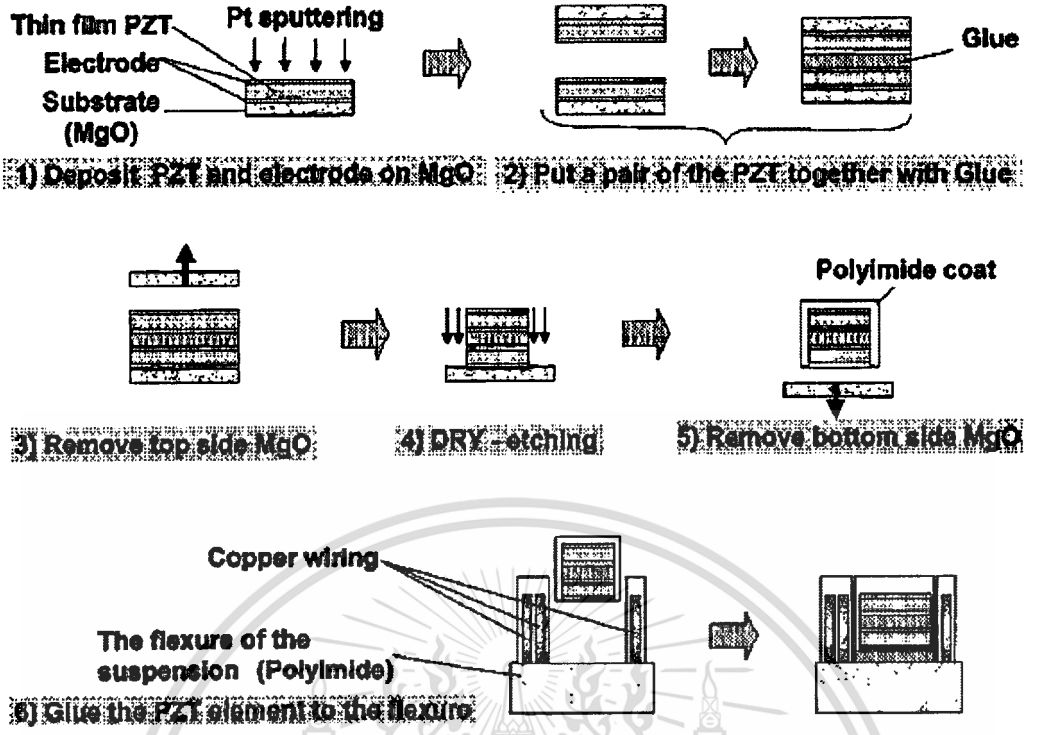

Figure 1.4 Process Flow of microactuator fabrication

[3] Mark D. Bedillion, Mahmut Karaman, and Patrick B. Chu Members, IEEE, "Spinstand Control Characterization of an Electromagnetic Slider Microactuator", American Control Conference, June 8-10, 2005, Portland, OR, USA

This paper is provided details modeling and servo control of an electromagnetic slider microactuator designed at Seagate and its promise as a solution for high accuracy tracking and positioning control. The device has passive high frequency windage disturbance attenuation due to its structure. Controller design is developed for a single stage spinstand environment used both PES feedback and feedback from a

piezo-resistive sensor that measures the motion of the slider relative to the suspension to show the device effectiveness as shown in Fig. 1.5 – 1.9.

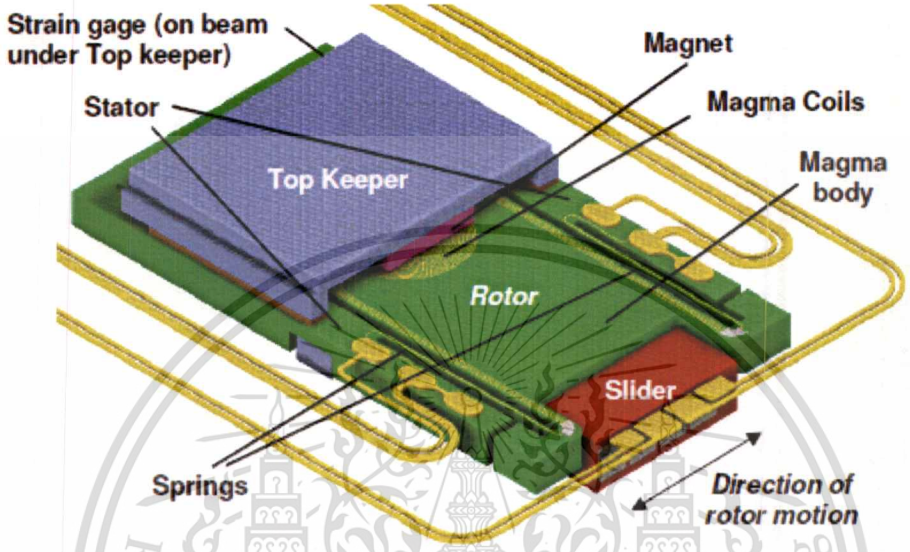

Figure 1.5 Top view of a MAGMA actuator CAD drawing

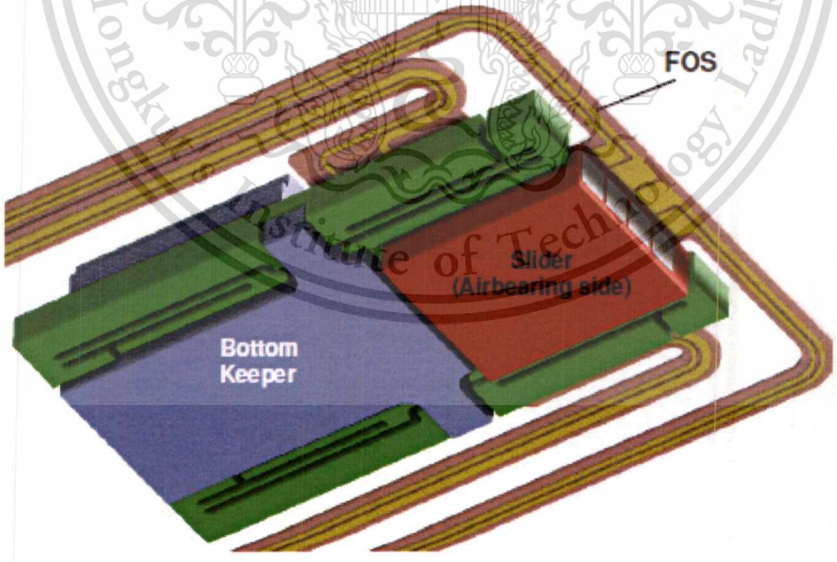

Figure 1.6 Bottom view of a MAGMA actuator CAD drawing

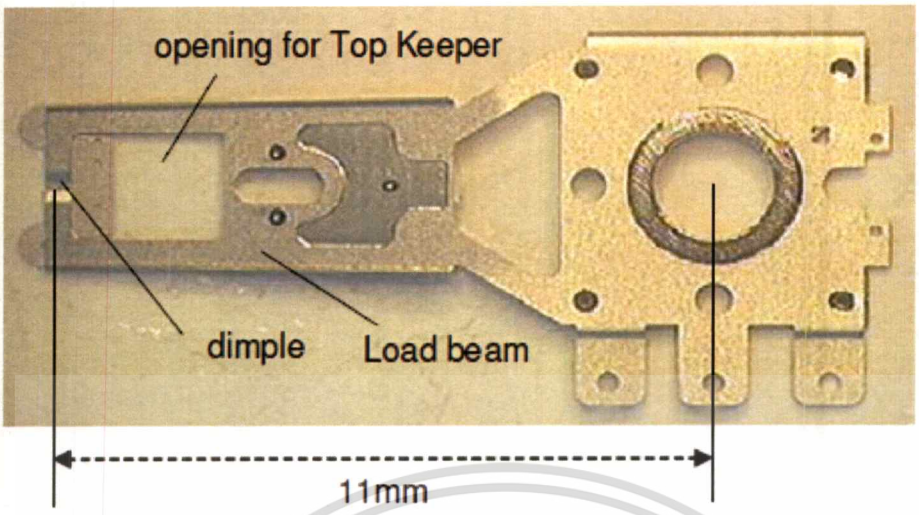

Figure 1.7 Photo of Custom suspension (Top view)

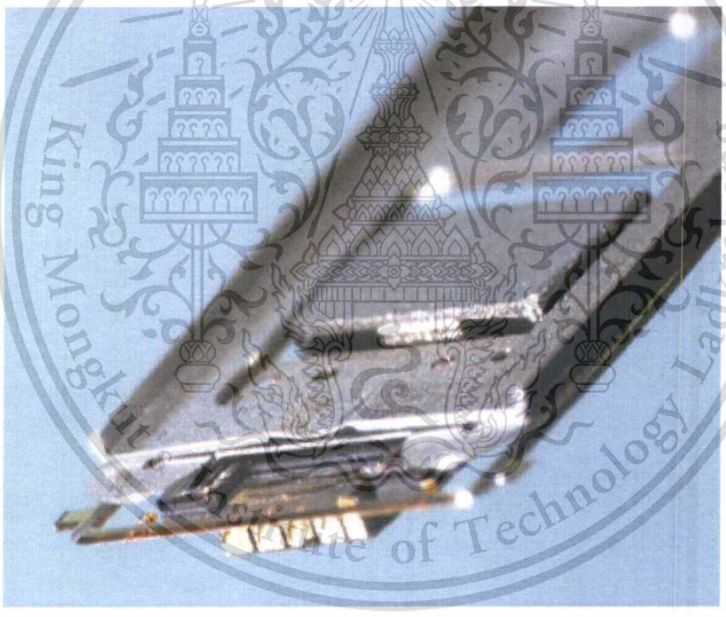

Figure 1.8 Photo of MAGMA on Custom suspension

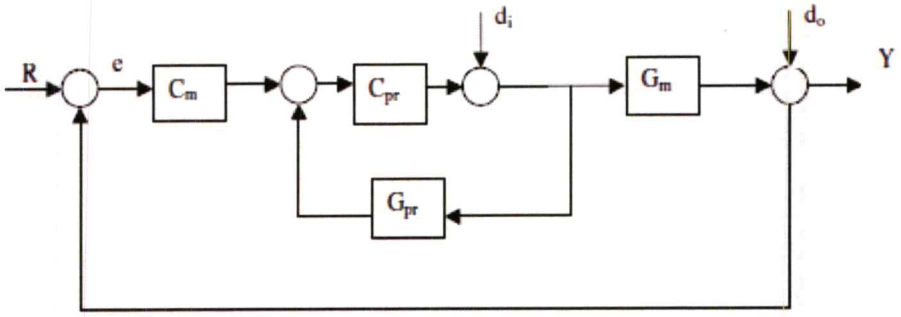

Figure 1.9 System Block Diagram

[4] Kwong Wah Chan, and Wei-Hsin Liao Smart Materials and Structures Laboratory, Department of Automation and Computer-Aided Engineering, The Chinese University of Hongkong, "Precision Positioning of Hard Disk Drives Using Piezoelectric Actuators with Passive Damping", Proceeding of the 2006 IEEE, International Conference on Mechatronics and Automation, June 25 – 28, 2006, Luoyang, China

This paper simulates and experiments prototype of three types of piezo-based dual-stage actuators for concept verification and feasibility study. The advantages of the EACL (Enhanced Active Constrained Layer) design are illustrated as compared to the ACL (Active Constrained Layer) and PA (Purely Active) configurations. It has been found that the EACL design can achieve minimum overshoot, fast settling, and fine precision during positioning as it possess good transmissibility and damping ability as shown in Fig. 1.10 – 1.15. The overall performance for EACL is the best among them.

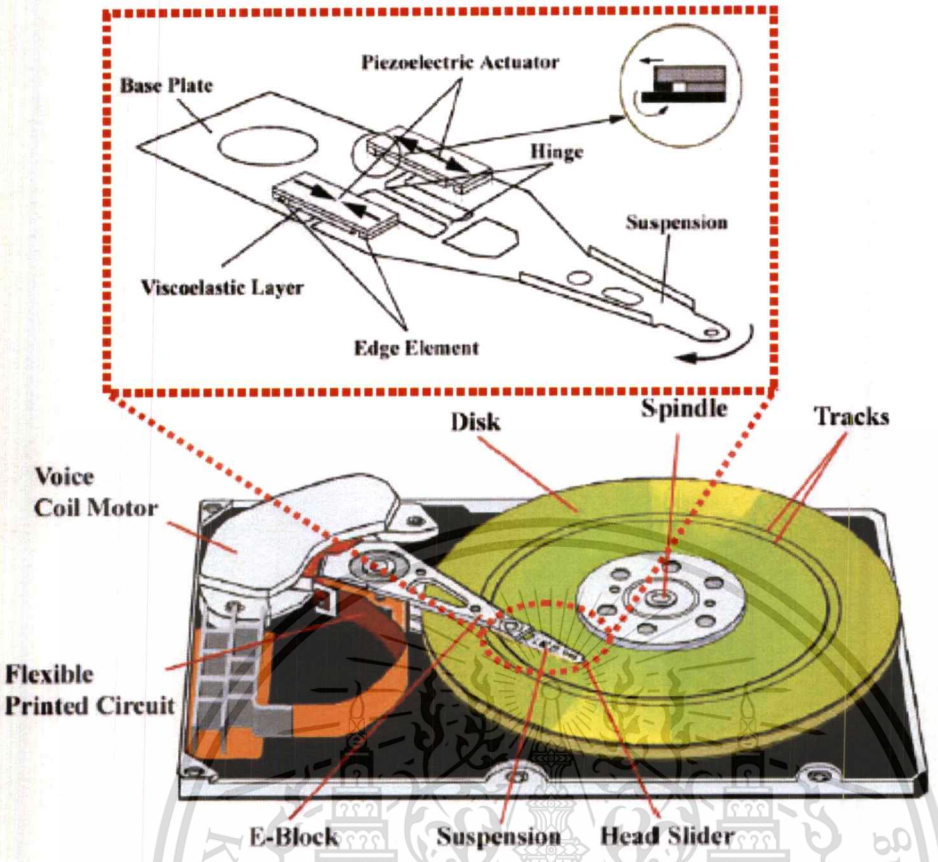

Figure 1.10 Schematic of a dual-stage servo system

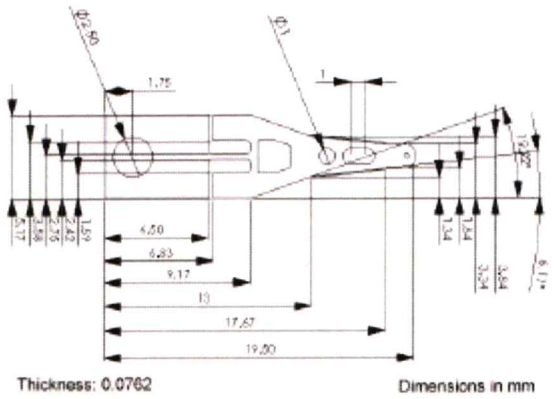

(a) Load beam (suspension)

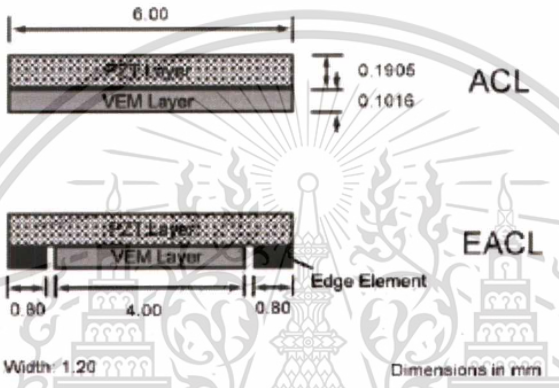

(b) Micro actuators

Figure 1.11 Dimensional of the load beam and microacuator

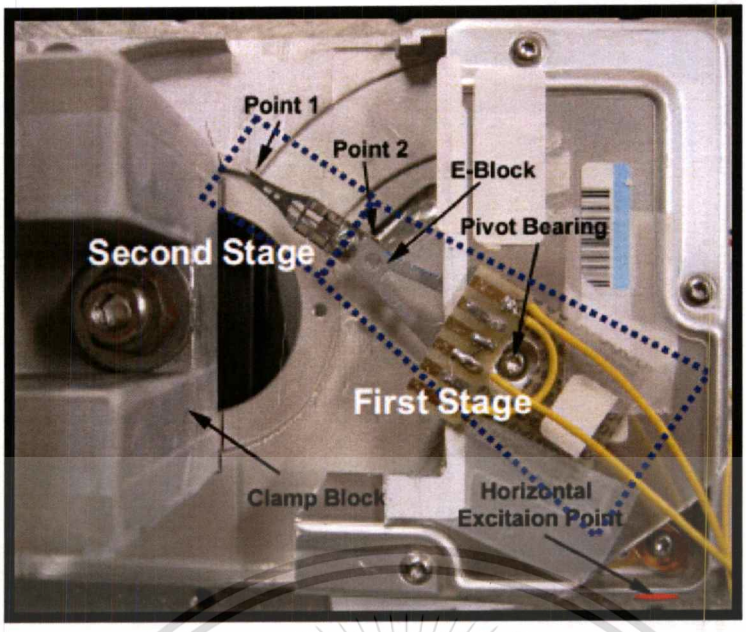

Figure 1.12 Micro actuators integrated with the voice coil motor

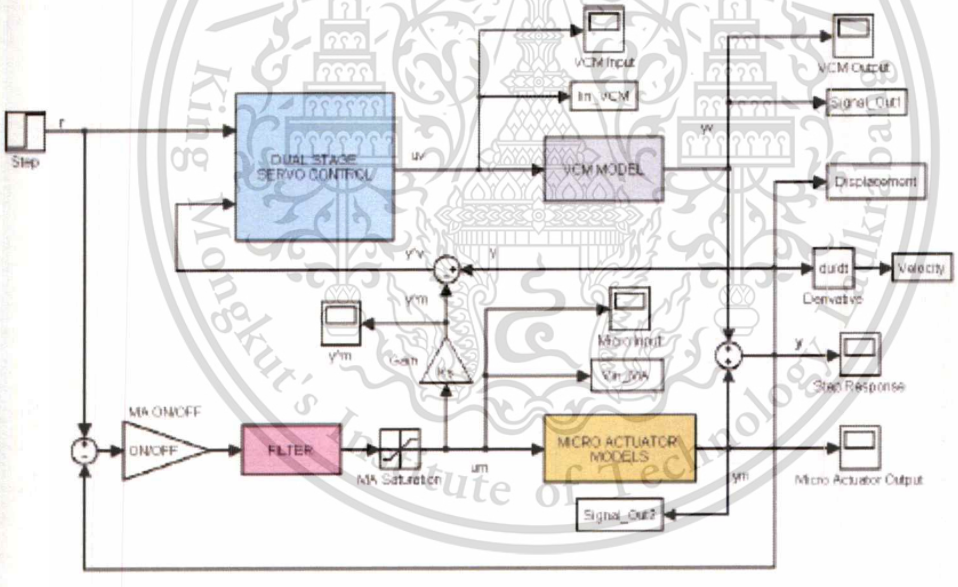

Figure 1.13 Block Diagram of the dual stage servo system with micro actuators

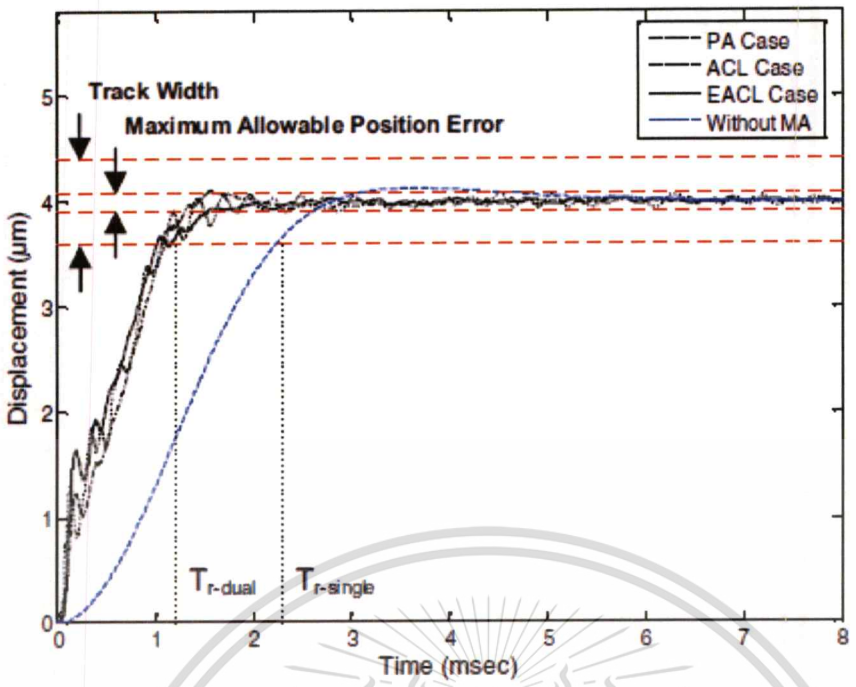

Figure 1.14 Step Responses for r = 4µm in track seeking

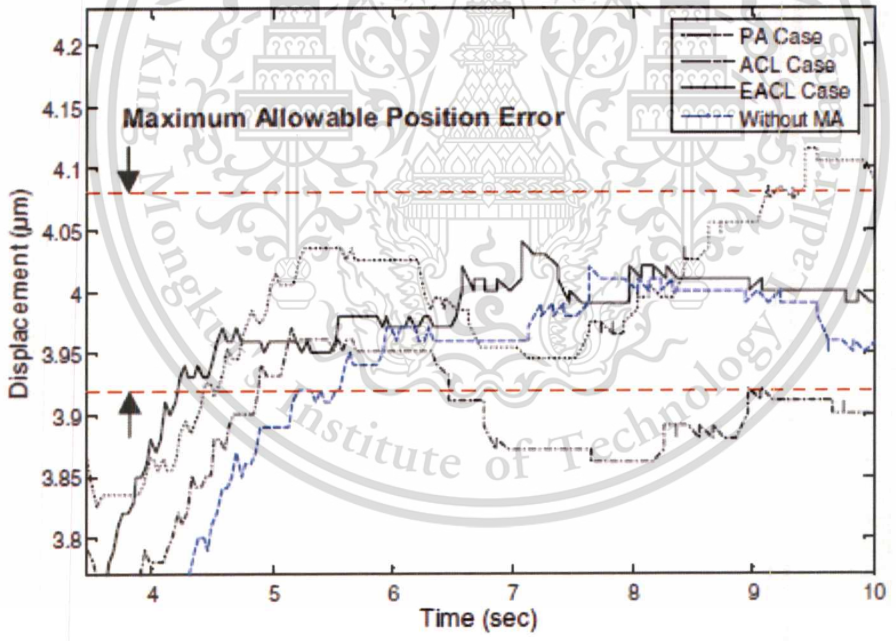

Figure 1.15 Measured track following in the allowable position error region

[5] K. Mori, T. Muneomoto, H. Otsuki, Y. Yamaguchi and K. Akagi "A dual-stage magnetic disk drive actuator using a piezoelectric device for a high track density", IEEE TRANSECTIONS ON MAGNETICS, VOL. 27, NO. 6, November 1991

This paper describes the design of dual-stage actuator including structural analysis, its static and dynamic characteristics, dual-stage feedback control system, and experimental results of tracking with high accuracy on a 3.5" disk-drive unit as shown in Fig. 1.16 – 1.17.

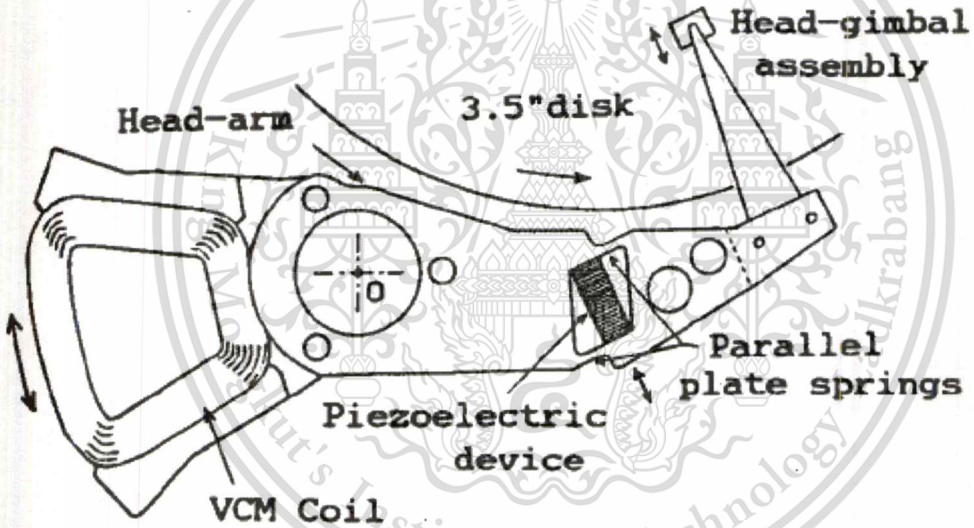

Figure 1.16 Structure of a dual-stage actuator

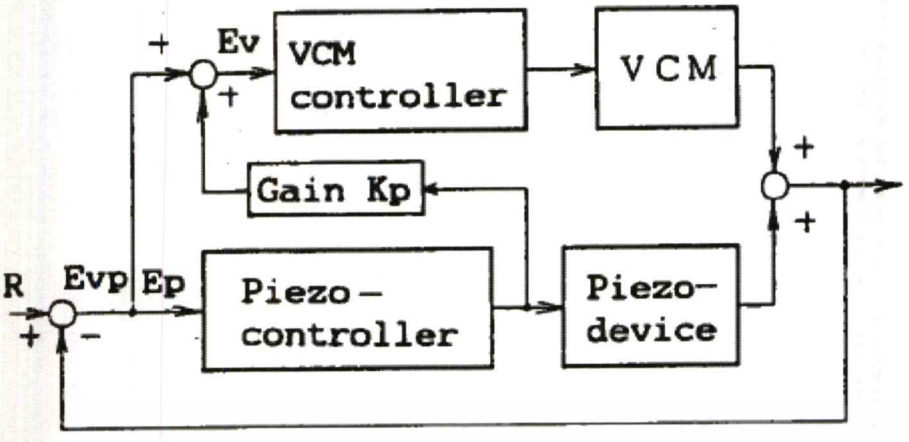

Figure 1.17 Block diagram of the dual-stage servo system

1.7 Thesis Organization

This thesis is organized in the following way manner. Chapter 2 presents the HGA Process in hard disk drive manufacturing; Chapter 3 presents the fundamental concepts of piezoelectricity; Chapter 4 presents design of experiment; Chapter 5 presents experiment results and Chapter 6 Conclusions. This research will be concluded and some importance issues for further work will be also given.

CHAPTER 2

HGA Process in HDD Manufacturing

Head Gimbal Assembly (HGA) process is the process to assemble the slider onto suspension by using adhesive as shown in figure 2.1. The HGA is one of the components in hard disk drive (HDD).

The HGA process flow is showed as figure 2.1 below

Figure 2.1 The HGA Process Flow

HGA is composed of slider and Trace Gimbal Assembly (TGA) as shown in figure 2.2. TGA is the suspension with circuit. HGA process is the process of attaching a slider onto TGA with curing adhesive and bonding or connecting between the gold bond pad on trailing end of

slider and the lead of TGA by using Thermal Inter Connect (TIC) jetting the solder to the pads.

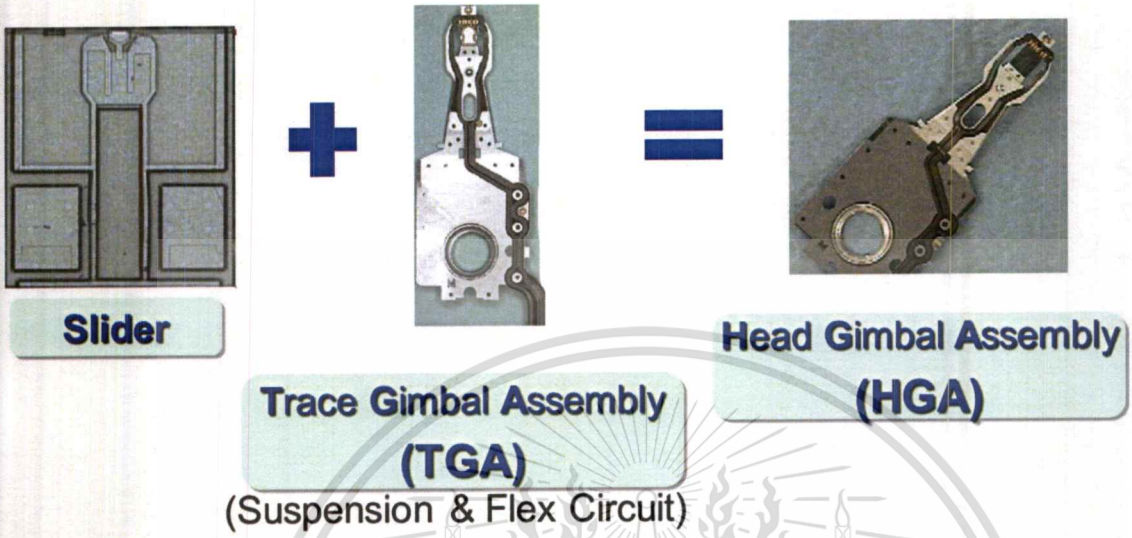

Figure 2.2 Head Gimbal Assembly and piece parts

2.1 Suspension Load

This is the first station for HGA Process to pick up suspension from suspension tray load onto Front of Line Assembly (FOLA) carrier and preparing to dispense adhesive on the gimbal area. The station will pick suspension from TGA tray and pre-align at nest for the right position prior to load to FOLA carrier. This is because if the position of the TGA not properly align, it will not load onto FOLA carrier and may cause suspension damage and bend problem. The suspension pre-align to the nest is very important.

2.2 Adhesive Dispense

This station is to dispense adhesive on the gimbal area of TGA. This step needs a precise control of adhesive dot size and dot location onto the TGA gimbal area. If the adhesive is not on the right position on TGA, it will cause the problem to the next station for attaching the slider onto the suspension. And if the adhesive dot size is bigger than the TGA gimbal area, it will over flow to the others area of suspension causing sticky contamination problem. If the adhesive dot size is too small (little amount), slider may not attach well (poor bonding strength) and can be falled off/loosened from the gimbal bonding area. The adhesive dot size is needed to be monitored. Once it put the adhesive dot onto the TGA gimbal area, it will pre-heat the adhesive dot on suspension prior to move to the next station. Otherwise, adhesive will spread and flow onto the other area.

2.3 Slider Attach

This station is to attach the slider onto the suspension by using adhesive. After dispense adhesive onto the TGA gimbal area, the station will pick up slider from the slider pocket in slider tray and move to nest to read the wafer code and record/send the data to Radio Frequency Identification (RFID) on FOLA carrier and to database. Then the station will pick and move slider to attach onto the suspension. This step need to control alignment of slider on the TGA that may effect to the recording head (write and read) process and flying performance above media.

2.4 Adhesive Cure

This station is to cure the adhesive by using Thermal (Conventional) or Infrared Radiation (IR) oven (It depends on the process/product design/requirements). This station needs to control temperature and time for curing the adhesive. The suspension with slider attached from the previous station will be loaded onto this station by FOLA carrier and conveyor. The oven will cure the adhesive per temperature and time setting on machine per process/product design/requirements. After curing, HGAs are sampled to check the bonding strength by the gimbal bond shear tester to shear slider and suspension. Also some sampled to check the slider alignment with suspension by pinnacle machine. The pinnacle machine will measure X-Y and Z alignment for slider position on the suspension.

2.5 Interconnect

This station is to connect the gold bond pad of the slider to the lead (circuit) pad of the TGA by Thermal Inter Connect (TIC) with solder. This step needs to control the bonding parameters such as temperature, time (depending on product/process design/requirements and TIC machine) to get the good circuit connection.

2.6 Visual Inspection

This station is to inspect the mechanical defects under microscope to screen the defected parts out, such as bent flexture, bent gimbal, contamination, bridging on bonding pad (short circuit) and

discolor for Piezoelectric (PZT). This inspection operation may sample to monitor mechanical problem from assembly process steps. If the defected part is found, production line must stopped and find out the root cause of problem prior to resuming the process and may need to screen out bad parts from the HGA Process.

2.7 HGA Unload

This station is to unload HGA from Front of the line Automation (FOLA) carrier and load onto Back of the Line Automation (BOLA) tray. The HGA BOLA process steps consist of Cleaning, Pitch and Roll Static Attitude (PSA & RSA) Measure and Adjust, Electrical Test, Spring Measurement, FLY Measurement, Tail Fold and Final Visual Inspection.

2.8 HGA Cleaning

This station is to clean HGA from assembly process prior to move to the next step. Due to HGA pass thru many operations and may have particles or contamination on itself, to ensure HGA parts are cleaned prior to move to electrical testing. HGA will be cleaned by aqueous cleaning machine should be optimized and controlled to get the high efficiency cleaning for HGA cleanliness, such as ultrasonic power, time, frequency and temperature.

2.9 Pitch and Roll Static Attitude (PSA/RSA) Measure and Adjust

This station is to measure the angular relationship of HGA on Air Bearing Surface (ABS) that mounted onto the suspension. If the PSA and

RSA do not meet the product requirements, it will adjust the angular relationship of both PSA and RSA to be on the target, if not rejected parts. Both PSA and RSA are also effect read/write process performance and the flying height of recording head over the media.

2.10 Electrical Test

This station is to perform electrical test of the recording head parameters including write performance (ability to write the data) such as track average amplitude, overwrite, signal-to-noise ratio, bit error rate, pulse width at 50% and Stroke (PZT positioning) test by applying current and test above spinning media (dynamic test). The result of test can identify and separate good and bad HGA parts. The good HGA parts can be separated to be many sorts (grade) depending on customer requirement by grading the specification of each electrical parametric test.

2.11 Spring Measurement

In this station, HGA is sampled to measure the gram force. This test is to ensure that HGA can fly over the media within its fly height product requirement. If HGA gram force too low causing fly over media too high, the distance between head and media will be too far and may effect on read/write process performance. If HGA gram force too high causing fly over media too low, head may touch and scratch onto the media. Both cases are caused both head and media damaged.

2.12 FLY Measurement

In this station, HGA is sampled to measure the head flying over the glass media. Both PSA/RSA and Spring measurement are the most critical to fly height performance and will affect for recording head read/write performance.

2.13 Tail Fold

This station is to fold the tail of TGA trace for putting in arm of Head Stack Assembly (HSA) process.

2.14 Final Visual Inspection

This station is to inspect the mechanical defects under scope to screen out the defected parts out, such as bent radius, bent flexture, bent gimbal, contamination and PZT discolor. This station is the last station prior to send it to HSA line to ensure no mechanical damaged to HGA.

CHAPTER 3

Fundamental Concepts of Piezoelectricity

The Areal density of magnetic disk drives has been increasing by about 30 to 60% every year. The track pitch is expected to become less than 1μm early in the next century [6]. The ultra-high positioning nano scale for head sensor and media track are required to get more accurate data in hard disk drive manufacturing process. The new suspension design with piezoelectric was proposed and developed [3].

Piezoelectricity is the electric charge that accumulates in certain solid materials (notably crystals, certain ceramics, and biological matter such as bone, Deoxyribonucleic Acid (DNA) and various proteins) in response to applied mechanical stress. The word piezoelectricity means electricity resulting from pressure. It is derived from the Greek piezo or piezein, which means to squeeze or press, and electric or electron, which stands for amber, an ancient source of electric charge. Piezoelectricity was discovered in 1880 by French physicists Jacques and Pierre Curie [7].

3.1 Piezoelectric effect

The piezoelectric effect is understood as the linear electromechanical interaction between the mechanical and the electrical state in crystalline materials with no inversion symmetry. The piezoelectric

effect is a reversible process in that materials exhibiting the direct piezoelectric effect (the internal generation of electrical charge resulting from an applied mechanical force) also exhibit the reverse piezoelectric effect (the internal generation of a mechanical strain resulting from an applied electrical field). For example, lead zirconate titanate crystals will generate measurable piezoelectricity when their static structure is deformed by about 0.1% of the original dimension. Conversely, those same crystals will change about 0.1% of their static dimension when an external electric field is applied to the material. The inverse piezoelectric effect is used in production of ultrasonic sound waves [8].

The piezoelectric material for this research is made from ferroelectric ceramic. Ferroelectricity is a property of certains material that have a spontaneous electric polarization that can be reversed by the application of an external electric field. Ferroelectric ceramics can be made piezoelectric (poled) below Curie temperature (T_C) by application of electrical field (E) greater than Coercive field (E_C). Ferroelectric materials posses a local spontaneous polarization which can be reoriented between two or more equivalent crystallographic directions under application of a DC electric field. Poling process aligns domains in the direction of the applied field yielding a net remnant polarization (P_R). Piezoelectric materials can be polarized by application of an electric field and also by application of mechanical stresses.

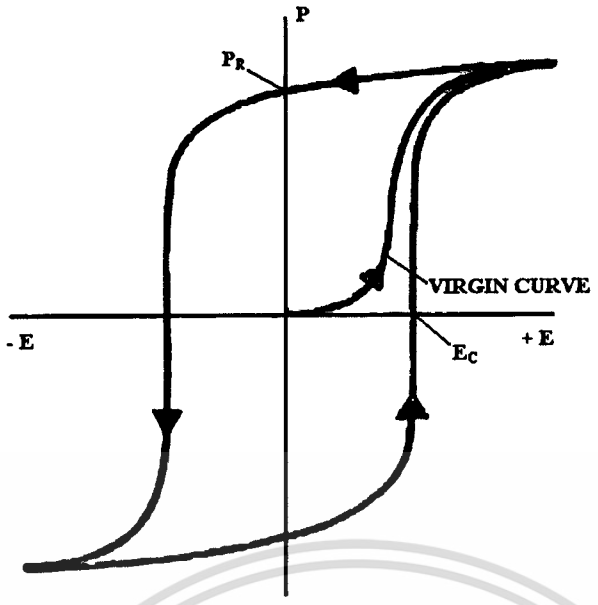

Figure 3.1 Charge-field hysteresis loop for ferroelectric materials

3.2 Ferroelectric polarization

Ferroelectricity can be verified through polarization of the material by application of electric field. The most important characteristic of ferroelectric material is switching of polarization. Figure 3.1 shows the typical charge – field hysteresis loop for ferroelectric materials. With the application of increasing field domains start orienting in the direction of field, extreme ends of the hysteresis loop (tail) represent the saturation where most of the domains are aligned in the direction of the applied field. Even after decreasing the field strength to zero all domains will not go back to original position, some domains will remain aligned in the positive direction. That is called as remnant polarization (P_R). When the field is applied in opposite direction, the dipoles reverse their orientation and then saturate in other direction. Field in negative direction when all domains are back to original position (zero

polarization) is called coercive field (E_C). The relation between polarization (P) and electric field (E) is represented by hysteresis loop. Experimentally ferroelectric hysteresis loop can be observed using Sawyer-Tower circuit [9].

The piezoelectric effect includes two types of responses; direct and converse. Production of electric charge when stress is applied is known as direct piezoelectric effect whereas the production of stress and/or strain when an electric field is applied is known as converse piezoelectric effect. Figure 3.2 shows the schematic illustration for direct and converse piezoelectric effect.

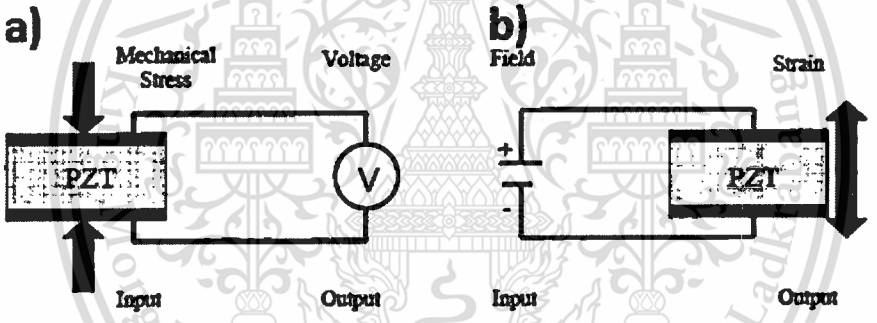

Figure 3.2 Schematic for a) Direct and b) Converse piezoelectric effect

3.3 Polycrystalline Ceramics Piezoelectric

Crystal structure is very important for the performance of piezoelectric ceramics. Piezoelectricity is related to lack of a center of symmetry. Crystal structures can be divided into 32 point groups, 21 of

them are noncentrosymmetric and 20 are piezoelectric. Under the application of homogeneous stress materials which lack a center of symmetry observe a net movement of positive and negative ions with respect to each other developing an electrical polarization proportional to an applied stress.

The main breakthrough in the field came in the mid 1900's with the synthesis and characterization of materials with perovskite structure [10]. Large numbers of technologically important piezoelectric materials crystallize in the perovskite structure. Two of the most interesting piezoelectric materials selected for aging study are lead zirconate titanate $(1\text{-}X)PbZrO_3\text{-}xPbTiO_3$ or PZT and Bismuth scandium – lead titanate $(1\text{-}x)BiScO_3\text{-}xPbTiO_3$ or BSPT belong to perovskite family.

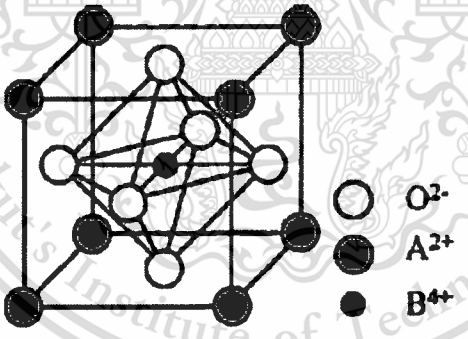

Figure 3.3 Perovskite ABO_3 unit cell[12]

The perovskite structure applies to series of compounds with three types of atoms with general formula ABO_3 described by a simple cubic unit cell with oxygen atoms at the face centers, larger cations at the cube corners (A sites) and smaller cations in body center(B sites).

Typical perovskite ABO_3 unit cell is shown in Figure 3.3 [11]. There are many complex perovskites which can be describe with the formula $(A',A'')^{XII}(B', B'')^{VI}O_3$, where XII and VI represent coordination numbers. In PZT, Pb^{2+} ions are situated at the corner of the unit cell (A sites), Zr4+ or Ti4+ at body center positions (B site). In BSPT, Pb^{2+} and Bi^{3+} share the A sites whereas Ti^{4+} and Sc^{3+} share the B sites. In both material O^{2-} is situated at face center position forming octahedra around the B site (BO_6).

Ideal perovskite structure is simple cubic lattice. Depending on the ionic radii of cations and anions the perovskite unit cell may be distorted to rhombohedral or tetragonal symmetry.

In polycrystalline ceramics piezoelectric and dielectric properties are depend on both intrinsic and extrinsic mechanisms. Intrinsic contributions are due to relative shift between cation and anion. When a voltage is applied to the perovskite unit cells one or more of the cations move due to the local field. Displacement of the cations with respect to oxygen octahedra causes distortion of the individual unit cell resulting strain in the piezoelectric material. This strain is typically ~ 0.2% for high performing polycrystalline ceramics whereas single crystals may strain >1%. Displacement of the central atoms can only occur in certain crystallographic directions depending on the type of structure i.e. tetragonal or rhobohedral.

Extrinsic contributions are mainly due to presence of domain walls and defect dipoles and those are thermally activated [13]. Depending on the relative orientation between polarization directions in neighboring domains there 180° and non-180° domain walls. A schematic representation of 180° and non-180° domain walls is shown in Figure 3.4. Ferroelectric domain walls may move under weak or moderate fields. The movement of domain walls due to external field affects the polarization and influences the piezoelectric and dielectric properties of ferroelectric materials. Both 180° and non-180° domain wall motion influences the changes in polarization, while only non-180° domain wall motion influences the strain output. The real ferroelectric ceramics always contain imperfections, electrical and eleastic defects. These imperfections and defects may cause pinning and clamping of domain walls [14].

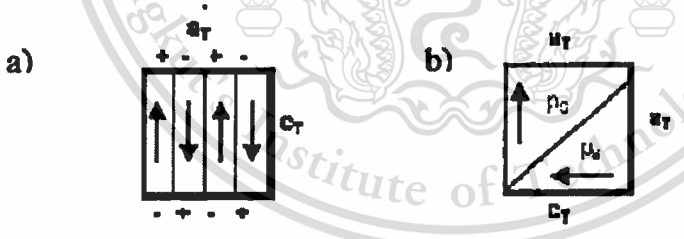

Figure 3.4 a) 180^0 and non-180^0 b) domain walls in tetragonal unit cell[14]

The most important piezoelectric material lead zircronate titanate $(1-x)PbZrO_3.xPbTiO_3$ or PZT was developed in 1950's, since then it is

been the dominant piezoelectric ceramic in the commercial market [15,16]. The high electromechanical properties, and Curie temperature and ability to tailor properties make this material suitable for wide range of applications. Commonly, used PZT 5A has Curie temperature T_C ~365^{0}C and piezoelectric coefficient d_{33} 375pC/N [17].

In PZT depending on the % of Zr^{+4} or Ti^{+4} the crystal structure is either rhombohedral or tetragonal. Figure 3.5, shows the temperature-composition phase diagrams for PZT system [18]. At room temperature Zr rich region has rhombohedral structure (F_R) with two space groups *R3m* and *R3c*, and Ti rich region has tetragonal structure (F_T) with space group *P4mm*. In rhombohedral phase the polarization whereas in tetragonal phase polarization is parallel to the edges of the unit cell and has six equivalent state of polarization. The line separating two regions called morphotropic phase boundary (MPB) which is about x 0.48. PZT has nearly vertical MPB. Traditional understanding is that compositions near the MPB have coexistence of rhombohedral and tetragonal phase to give 14 possible polarization directions to optimize crystallographic orientation and resulting high dielectric and piezoelectric properties.

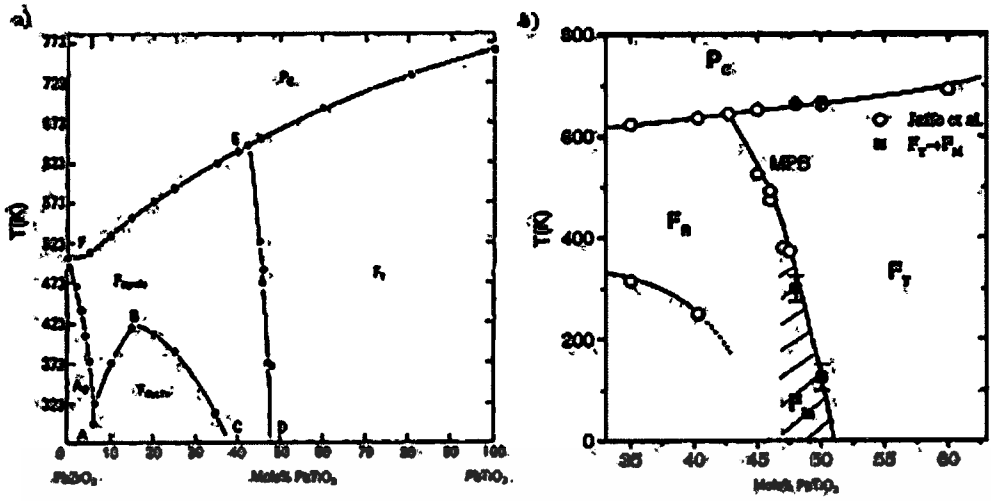

Figure 3.5 Temperature – composition phase diagram for PZT a) after Jaffe et al. 1971 and b) modified by B. Noheda, 2000[18]

Recently, Noheda et al, 2002 reported the presence of the monoclinic structure (F_M) with space group *Pc* at the MPB [19]. PZT has the cubic structure at high temperatures; the cubic to tetragonal phase transformation takes place at 660 K for MPB composition. The tetragonal to monoclinic phase transformation was discovered at 300K. The monoclinic unit cell is rotated 45° about c axis with respect to tetragonal cell, a_m and b_m lie along the tetragonal face diagonals [110] and [110] directions and c_m deviates slightly from [001] direction.

3.4 Piezoelectric Ceramic Fabrication Process

The fabrication of most bulk piezoelectric ceramics starts with powder preparation. The powder is then processes to the required shapes and sized, and the green shapes are in turn processed to mechanically strong and dense ceramics. The more important processes

that influence the product characteristics and properties are powder preparation, powder calcining and sintering. The next step are miching, electroding and poling: application of a DC field to orient the dipoles and induce piezoelectricity.

The most common powder preparation is the mixed oxide route. In this process, powder is prepared from the appropriate stoichiometric mixture of the constituents' oxides. In the case of lead zirconate titanate (PZT): lead oxide, titanium oxide, and zirconium oxide are the main compounds. Depending on application, various dopants are used to tailor the properties of interest. PZT ceramics are rarely utilized without the additional of dopants to modify some of their properties. A-site additives tend to lower the dissipation factor, which affects heat generation, but also lower the piezoelectric coefficients; for this reason they are mostly used in ultrasonics and other high frequency applications. B-site dopants increase the piezoelectric coefficients but also increase the dielectric constant and loss. They are utilized as actuators in vibration and noise control, benders, optical positioning application etc.

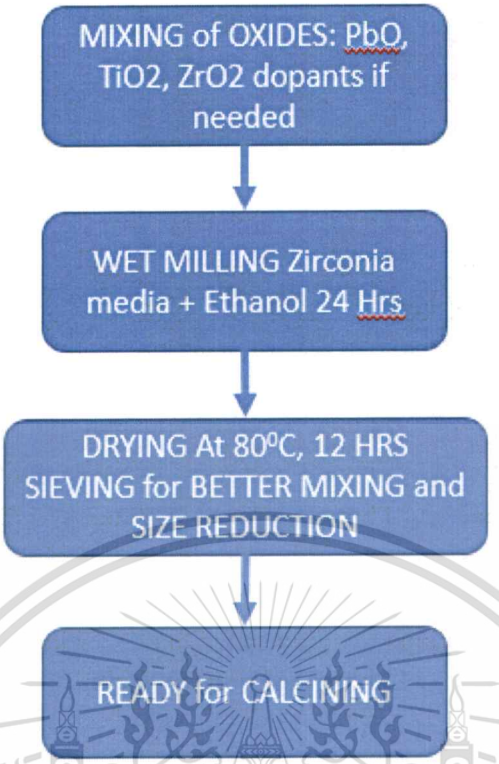

Figure 3.6 Mixed-Oxide route of preparing PZT

Figure 3.6 shows a flowchart of the mixed oxide route for making PZT ceramics. Mixing of the powders can be done by dry-ball milling or wet ball milling, both methods having advantages and disadvantages: wet ball-milling is faster than dry-milling; however, the disadvantage is the added step of liquid removal. The most common method for making PZT ceramics is through wet-ball milling; ethanol and stabilized zirconia media are added for a wet milling process. A vibratory mill may be used rather than a conventional ball mill; it was shown by Herner [20] that this process reduces the risk of contamination by the balls and the jar. Zirconia media are used to further reduce the contamination

risks. The calcination step is a very crucial step in the processing of PZT ceramics; it is important that the crystallization be complete and that the perovskite phase forms during this step. The goals are to remove any organics, water or other volatiles left after mixing; to react the oxides to form the desired phase composition before the ceramics is processed to useful devices; and to reduce volume shrinkingage and allow for better homogeneity during and after sintering.

After calcining, a binder is added to the powder, then the mixture is shaped usually by dry-pressing in a die for simple shapes, or extrusion, or casting for more complicated bodies. Next, the shapes are sintered: placed in an oven for binder burn-out and densification.

The major problem in the sintering of the PZT ceramic is the volatility of PbO at about 800^0C. To minimize this problem, the PZT samples are sintered in the presence of the lead source, such as PbZrO3, and placed in closed crucibles. The saturation of the sintering atmosphere with PbO minimizes lead loss from the PZT bodies. Sintering can now be carried out at temperatures varying between 1200-1300^0C. Despite precautions, there is usually a resulting loss of 2%-3% of the initial lead content.

After cutting and machining into desired shapes, electrodes are applied and a strong DC field is used to orient the domains in the polycrystalline ceramics. DC poling can be done at room temperature

or at higher temperatures depending on the material and the composition. The poling process only partially aligns the dipoles in a poly crystalline ceramic, and the resulting polarization is lower than that for single crystals.

This processing technique presents many uncertainties and the presence of a wide number of other fabrication techniques is an indication that there is a great need for the production of reliable PZT ceramics with optimum properties and microstructure. One problem often encountered is the deviation from stoichiometry. This problem is often due to impurities present in the raw material as well as the lead loss during the sintering process, which invariably results in substantial alterations of the PZT properties. As a result, the elastic properties can vary as much as 5%, the piezoelectric properties 10% and the dielectric properties 20% within the same batch [21]. Also, the piezoelectric and dielectric properties generally suffer if there is any lack of homogeneity due to poor mixing. It is constituents are solid solutions and it has been shown that an intimate mixing of solid solutions is difficult if not impossible. More information on the preparation of piezoelectric ceramics can be found in Jaffe, Cook and Jaffe [1], and Moulson and Herbert [22] among others. Other processing methods including hydrothermal processing and co-precipitation methods are described in references [23-25]. It is noted that there has been a great deal of development in powder processing, shaping and sintering [26-28] that

has resulted in further expanding the application of piezoelectric ceramics.

3.5 Performance of Piezoelectric Device

The performance of piezoelectric devices depends on various electromechanical properties. Some of the important properties of piezoelectric material are ferroelectric Curie temperature (T_C), piezoelectric constant (d), dielectric constant (K) and loss (D or tan δ) and electromechanical coupling coefficient (k). Typical properties for various PZT and BSPT materials are given in Table 1.1. Shrout et al. 2007 showed that general piezoelectric properties of a ferroelectric ceramic can be expressed with a simple mathematical equation (3.1),

$$d_{ij} \sim 2\, Q_{ij}\, K\, \varepsilon_0 Pi \qquad (3.1)[17]$$

where d_{ij} is the piezoelectric constant, P_i the remnant polarization, K the dielectric constant, ε_0 the permittivity of free space, and Q_{ij} the electrostrictive coeffient. Since Q_{ij} exhibit little temperature dependent below Curie temperature T_C. the perovskite ferroelectric ceramics with high piezoelectric constant d_{ij} also exhibits high dielectric constant K. Within the lead base piezoelectric family, materials with low ferroelectric Curie temperature T_C exhibit high piezoelectric and dielectric properties. The reduction of ferroelectric Curie temperature is also associated with high thermal dependence of properties, and high aging rates. As a rule of thumb, piezoelectric ceramics can be used safely

to ~½ T_C (^{0}C) without much change in piezoelectric properties. Hence engineering of piezoelectric ceramics is always an optimization of piezoelectric and dielectric ceramics is always an optimization of piezoelectric and dielectric properties and also ferroelectric Curie temperature T_C.

Table 3.1 Electromechanical properties of PZT and BSPT materials

Material	Curie point (^{0}C) T_C	Dielectric Constant (1Khz) K	Dielectric loss (1Khz) D	Piezoelectric constant (10^{-12} C/N) d_{33}	Electromechanical coupling coefficient k_{33}
$Pb(Zr_{0.52}Ti_{0.48})O_3$ [3]	386	730	0.004	223	0.67
Hard PZT – 5H [52]	190	3400	0.02	590	0.75
Hard PZT- 8 [52]	300	1000	0.004	225	0.64
Hard PZT- 4 [52]	328	1300	0.004	290	0.70
Hard PZT PCM-40 [33]	325	1250	0.003	290	0.67
Hard PZT PIC 181 [34]	330	1200	0.003	265	0.66
Soft PZT- 5A [52]	365	1700	0.02	375	0.71
Soft PZT PCM-51 [33]	340	1850	0.019	405	0.74
Soft PZT PIC 151 [34]	250	2400	0.02	500	0.69
BSPT 64 [41,50]	450	2010	0.05	460	0.56
BSPT 66 [41]	460	1370	0.03	260	0.43
BSPT 64 + Mn [48]	445	1540	0.01	390	0.69
BSPT 66 + Mn [48]	468	1112	0.01	270	0.65

Ferroelectric materials posses a local spontaneous polarization and shows hysteresis relation between polarization and applied electric field. This behavior is observed in certain temperature region which depends on the transition of ferroelectric phase to paraelectric phase. Temperature above which the material loses its spontaneous

polarization and piezoelectric characteristics is know as ferroelectric Curie temperature (T_C).

Depending on composition PZT has rhombohedral, tetragonal or mixed perovskite structure below T_C and shows net dipole moment due to displaced central cation (Zr^{4+} or Ti^{4+}). Above T_C the material is cubic and the central cation is no longer displaced from the centre of the unit cell, leaving no net dipole moment and no spontaneous polarization.

As the temperature is increased, near T_C the dipoles have the tendency to revert back to random orientation. Degradation of piezoelectric properties due to loss of polarization is called thermally activated aging. In order to minimize the aging effect, maximum applications of materials are restricted to ~½ T_C. PZT has T_C ~386^{0}C and shows rapid degradation above ~200^{0}C. Recently, developed BSPT system has T_C ~450^{0}C and are much more stable at temperature higher than 200^{0}C [29-30].

As discussed in section 3.1, the piezoelectric effects include two type of responses; direct and converse. The basic mathematical equations (3.2) and (3.3) describe the above two types of piezoelectric effects are,

$$D = d \cdot T \qquad \text{(Direct piezoelectric effect)} \qquad (3.2)$$

$S = d \cdot E$ (Converse piezoelectric effect) (3.3)

Where D is the dielectric displacement, T the stress, S the mechanical strain, E the electric field, and d the piezoelectric constant which is numerically constant for both effects. Piezoelectric properties are also anisotropic and vary with direction of polarization axis and strain, hence may be specificed in tensor form as in equation (3.4) to indicate directionaly.

$$D_i = d_{ijk} \cdot T_{jk} \text{ and } S_{jk} = d_{ijk} \cdot E_i \quad (3.4)$$

Depending on the application, piezoelectric devices may use one of the above piezoelectric effects. High d is desirable for actuator applications like ultrasonic cleaner transducers, where materials are intented to develop motion or vibrations.

Another frequently used piezoelectric constant is g_{ij} which is related to d by equations (3.4).

$$g = d / \varepsilon = d / K \varepsilon_0 \quad (3.5)$$

where ε the dielectric permittivity of material, and ε_0 the dielectric permittivity of vacuum. High g is desirable for sensors applications like

pressure sensors, where material are intended to generate voltage in response to mechanical stress.

The relative dielectric constant K is the ratio of the complex permittivity ε of the material and the permittivity of free space ε_0 (8.85 X 10^{-12} F/m). Piezoelectric ceramics generally have a higher dielectric constant K, typical values for PZT and BSPT systems are 800 and as high as 2000 respectively.

$$K = \varepsilon / \varepsilon_0 \tag{3.6}$$

When an alternating voltage is applied to dielectric materials induced dielectric moment has both real and imaginary components, which is due to resistive leakage or dielectric absorption. The loss factor D is the ratio of imaginary component to the real component and expressed as equation (3.7)

$$D\ (\tan \delta) = \varepsilon'' / \varepsilon' = k'' / k' \tag{3.7}$$

Input energy to piezoelectric devices can be either in mechanical stress or electrical charge. The electromechanical coupling factor (k) is square root of the fraction of mechanical energy converted to electrical energy or vice versa. *k* is the material constant for piezoelectric crystals and it depends on degree of poling for ceramics.

$$k = \sqrt{\frac{Energy\ converted\ (mechanical\ or\ electrical)}{Energy\ applied\ (mechanical\ or\ electrical)}} \qquad (3.8)$$

Typical value of electromechanical factor for PZT and BSPT is in the range from 0.45 to 0.70.

CHAPTER 4

Design of Experiment

4.1 Motivation of experiment

The areal density of magnetic disk drives has been increasing by about 60% every year. The track pitch is expected to become less than 1um early in the next century. The ultra-high positioning nano scale for head sensor and media track are required to get more accurate data in hard disk drive manufacturing process. The new suspension design with piezoelectric was proposed and developed. During the new suspension design with piezoelectric launch and qualify, it was found that 100% of the new suspension failed stroke during applied voltage to the part, it does not move.

The piezoelectric theory and structure are very importance for further study in HGA manufacturing process. In the HGA manufacturing process has many steps as explained in details in Chapter 2 section 2.1 that may contribute to stroke failure at electrical testing operation. The electrical test data has been verified and invested including parts send to FA for higher magnification visual inspection, material and structural analysis.

Each HGA process steps must be investigated in micro process steps using multi-meter to measure capacitance and resistance change in each stations to identify the source of stressor. Further analysis on ET

tester is an important operation in HGA Process and mainly used for testing the electrical parametric performance of HGA.

4.2. Apparatus

Scanning Electron Microscope (SEM) is one of Failure Analysis (FA) equipments that can visually inspection on all stroke failures head with very high magnification to verify any mechanical damage to the PZT bonded area.

X-Ray machine is another of FA equipments that can visually inspect the failed parts to verify any mechanical damage to the PZT bonded area.

Multi-meter with nano probe for measuring capacitance of the stroke failure parts will be used for micro process mapping in HGA manufacturing process and to characterize the PZT performance without performing flying head over the recording media at Electrical Tester. Piezoelectricity is a linear effect that is related to the microscopic structure of the solid. Some ceramic materials become electrically polarized when they are stained; this linear and reversible phenomenon is referred to as the direct piezoelectric effect. The direct piezoelectric effect is always accompanied by the converse piezoelectric piezoelectric effect where a solid becomes strained when placed in an electric field. The microscopic origin of the piezoelectric effect is the displacement of ionic charges within a crystal structure. In the absence

of external strain, the charge distribution within the crystal is symmetric and the net electric dipole moment is zero. However, when an external stress is applied, the charges are displaced and the charge distribution is no longer symmetric. A net polarization develops and results in an internal electric field [31]. A material can only be piezoelectric if the cell has no center of inversion, so the multi-meter is considered to measure the capacitance and resistance of piezoelectric performance in HGA manufacturing process mapping tool.

Electrical Tester is recording head computerized test system that can measure and characterize the stroke failure parts. It can vary bias voltage to the part and measure head movement in each direction according to the bias voltage apply onto the parts.

Thermocouple and PICO gage are used to measure temperature at Slider Attach and Infrared Oven Cure Machine set up.

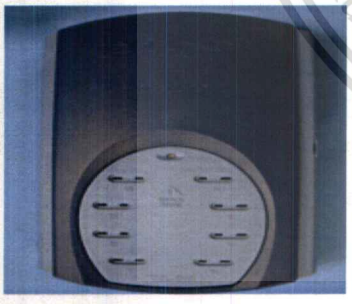

Pico Model TC-08

Thermocouple Wire Connector

Figure 4.1 Thermocouple and PICO gage for temperature measurement

The wave C is another tool that used to verify mechanical stroke measurement and characterize the PZT performance without performing flying head over the recording media at Electrical Tester.

4.3 Structure Characterization

Mechanical verification on stroke failure parts is the first step of this research. To verify and characterize the stroke failure parts whether is there any mechanical damage to the failure parts using X-Ray, SEM Inspection and Shear Test.

4.3.1 Equipment for verification

- X-Ray Machine
- SEM Inspection
- Shear Test

4.3.2 Verification Step

- Set the X-Ray machine to operate as normal
- Visually Inspect and take image both good parts and stroke failure parts for comparison at piezoelectric bonding area underneath piezoelectric
- Compare images result between good parts and stroke failure parts for all joint areas underneath piezoelectric
- Set the SEM machine to operate as normal
- Visually Inspect and take image both good parts and stroke failure parts for comparison at piezoelectric body and bonding area underneath piezoelectric

- Compare images result between good parts and stroke failure parts for all areas on piezoelectric body and joint areas
- Set the shear test to operate as normal
- Shear test piezoelectric at bonding areas both good parts and stroke failure parts
- Visually Inspect under Lower magnification scope (30X)
- Set the SEM machine to operate as normal
- Visually Inspect and take image both good parts and stroke failure parts for comparison at piezoelectric bonding areas both on suspension and piezoelectric

4.4 Electrical Properties Characterization

The HGA Process mapping and verification by each step of the head gimbal assembly is the key this research to identify which process step of head gimbal assembly causing stress to the piezoelectric. To verify and characterize each head gimbal process steps using multi-meter to measure capacity and resistance on the parts.

4.4.1 Equipment for verification

- Multi meter

4.4.2 Verification Step

- Set the Multi meter to operate as normal
- Measure the capacitance and resistance for stroke failure parts at position 1 and 2 per fig. 4.2

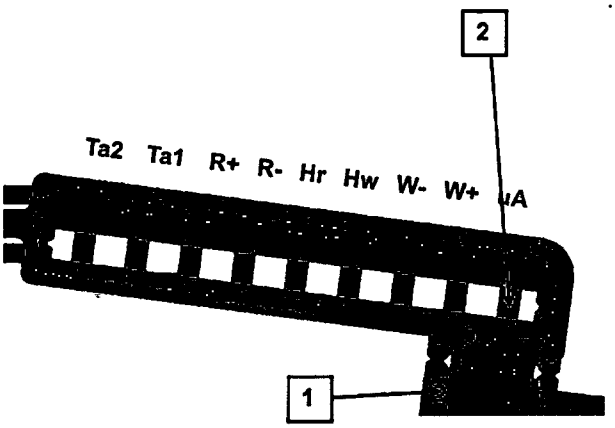

Figure 4.2 Measure Capacitance and Resistance

- Measure the capacitance and resistance at incoming parts (suspension level piezoelectric)
- Set the head gimbal process and each steps to operate as normal
- Build the measured suspension with capacitance and resistance reading along head gimbal process
- Compare Capacitance and Resistance result for all head gimbal process steps

4.5 Sources of Stroke failure inside the Infrared Oven

This experiment is to study and find sources of stroke failure inside the infrared oven cure station. The infrared oven is set and controlled for 10 parts per carrier. The infrared source is placed underneath parts and radiate close to gimbal bond area. There are 4 groups of Infrared Energy Level to be evaluated at 1.51, 2.51, 3.62 and 4.33 J/cm^2 and the current energy level at 3.14 J/cm^2. Sampling 50 TGAs at incoming

suspension and use multi-meter to measure capacitance for all TGAs and split into 4 groups.

4.5.1 Equipment for verification

- Multi meter
- Infrared Oven Cure Station
- Thermocouple and PICO gage

4.5.2 Verification Step

- Set Multi meter to operate as normal
- Measure capacitance for all TGAs group
- Set Infrared Energy level at IR Oven machine to operate as normal at 3.14 J/cm^2 for the control group (10 TGAs)
- Set Infrared Energy level at IR Oven machine at 1.51 J/cm^2 for the first group (10 TGAs)
- Measure capacitance for this group
- Set Infrared Energy level at IR Oven machine at 2.51 J/cm^2 for the 2'nd group (10 TGAs)
- Measure capacitance for this group
- Set Infrared Energy level at IR Oven machine at 3.62 J/cm^2 for the 3'rd group (10 TGAs)
- Measure capacitance for this group
- Set Infrared Energy level at IR Oven machine at 4.33 J/cm^2 for the last group (10 TGAs)
- Measure capacitance for this group

- Build all groups together until reach ET Test on the same tester
- Re-measure capacitance for all groups right after ET
- Compare capacitance for all groups in the table

4.6 Re-poling Piezoelectric Verification

This experiment is to study whether re-poling piezoelectric by applying an alternating voltage to dielectric materials will help degradation of piezoelectric properties by revert back to random orientation of the dipoles.

4.6.1 Equipment for verification

- Multi-meter
- DC Voltage Generator
- Cross section and SEM Inspection

4.6.2 Verification Step

Left piezoelectric

- Measure capacitance between 1 and 2 per Fig. 4.3

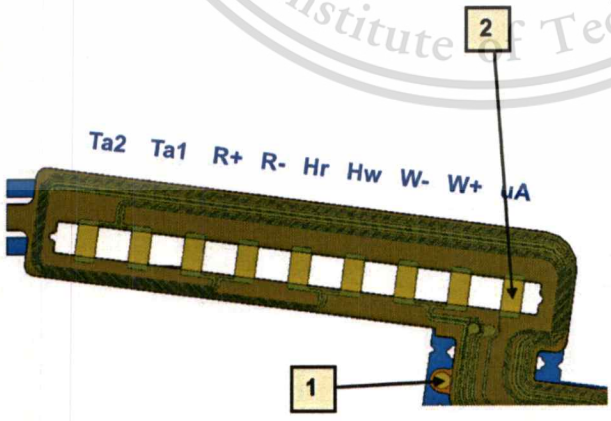

Figure 4.3 Capacitance measurement at 1 and 2

- Cut a trace as shown area E in Fig. 4.4

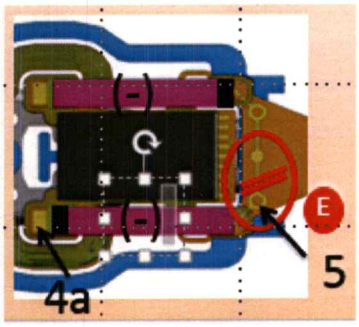

Figure 4.4 Cut a trace and measure capacitance at 4a and 5

- Measure a capacitance between 1 and 2 for left piezoelectric
- Measure a capacitance between 4a and 5 for right piezoelectric
- Applied DC voltage 92.5 V for 60 s between 1 (+) and 2 (-) for poling left piezoelectric is recommended by Seagate Suspension Design team in the US
- Applied DC voltage 92.5 V for 60 s between 4a (+) and 5 (-) for poling right piezoelectric is recommended by Seagate Suspension Design team in the US
- Measure a capacitance between 1 and 2 for left piezoelectric
- Measure a capacitance between 4a and 5 for right piezoelectric
- Connect the trace
- Measure capacitance between 1 and 2

  Right piezoelectric

- Measure capacitance between 1 and 2 per Fig. 4.5

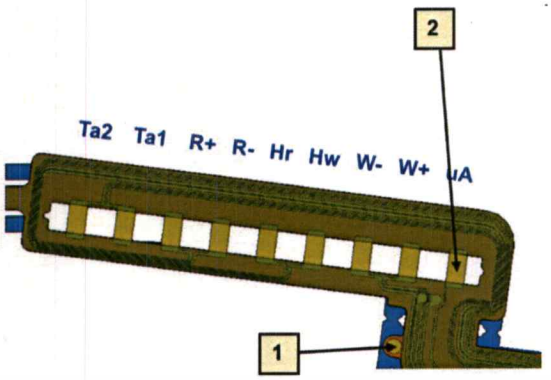

Figure 4.5 Capacitance measurement at 1 and 2

- Cut a trace as shown area D in Fig. 4.6

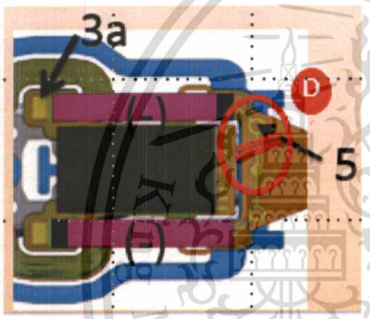

Figure 4.6 Cut a trace and measure capacitance at 3a and 5

- Measure a capacitance between 1 and 2 for right piezoelectric
- Measure a capacitance between 3a and 5 for left piezoelectric
- Applied DC voltage 92.5 V for 60 s between 1 (-) and 2 (+) for poling right piezoelectric is recommended by Seagate Suspension Design team in the US

- Applied DC voltage 92.5 V for 60 s between 3a (-) and 5 (+) for poling left piezoelectric is recommended by Seagate Suspension Design team in the US
- Measure a capacitance between 1 and 2 for right piezoelectric
- Measure a capacitance between 3a and 5 for left piezoelectric
- Connect the trace
- Measure capacitance between 1 and 2
- Take another set of stroke failure parts (5 HGAs)
- Measure mechanical stroke reading by using wave C
- Re-poling stroke failure parts per the above instruction
- Re-measure mechanical stroke reading on the same wave C
- Cross section and SEM inspection

4.7 Conclusion of Experimental Design

This chapter explains the experiment designs for this research. There are 4 main experimental designs setup and study. The first experiment is to verify mechanical damage or source of piezoelectric degraded due to any mechanical related using X-Ray, SEM with high

magnification and resolution for an external visual inspection and also shear test to verify the piezoelectric bonding condition and properly circuit connect to each others. The second experiment is to study the source of stressor in HGA manufacturing process and steps by using multi meter to measure capacitance and resistance each process steps. The third experiment is to study the source of stressor inside the IR Oven cure station by vary an infrared energy level. The current infrared energy level and another 4 levels of an infrared energy level are selected. The capacitance was measured after IR Oven process. The last experiment is to verify electrical performance of stroke failure parts after re-poling the piezoelectric properties back to the original dipoles orientation. Also verify by cross section and use SEM inspection after re-poling.

CHAPTER 5

Experiment Results

Mechanical and Electrical performance in each process step of head gimbal assembly is very importance and useful to identify the cause of stressor that can cause high stroke failure at electrical tester. Physical verification underneath piezoelectric at the bonding area is one of important thing to identify an abnormality of the failed parts. The information of sources and types of stressor will lead to find the root cause of stroke failure at electrical tester.

5.1 Structure Characterization

Mechanical verification on stroke failure parts is the first step of this research. To verify and characterize the stroke failure parts whether is there any physically damage to the failure parts from mechanical related issue using X-Ray, SEM Inspection and Shear Test.

5.1.1 X-Ray Inspection

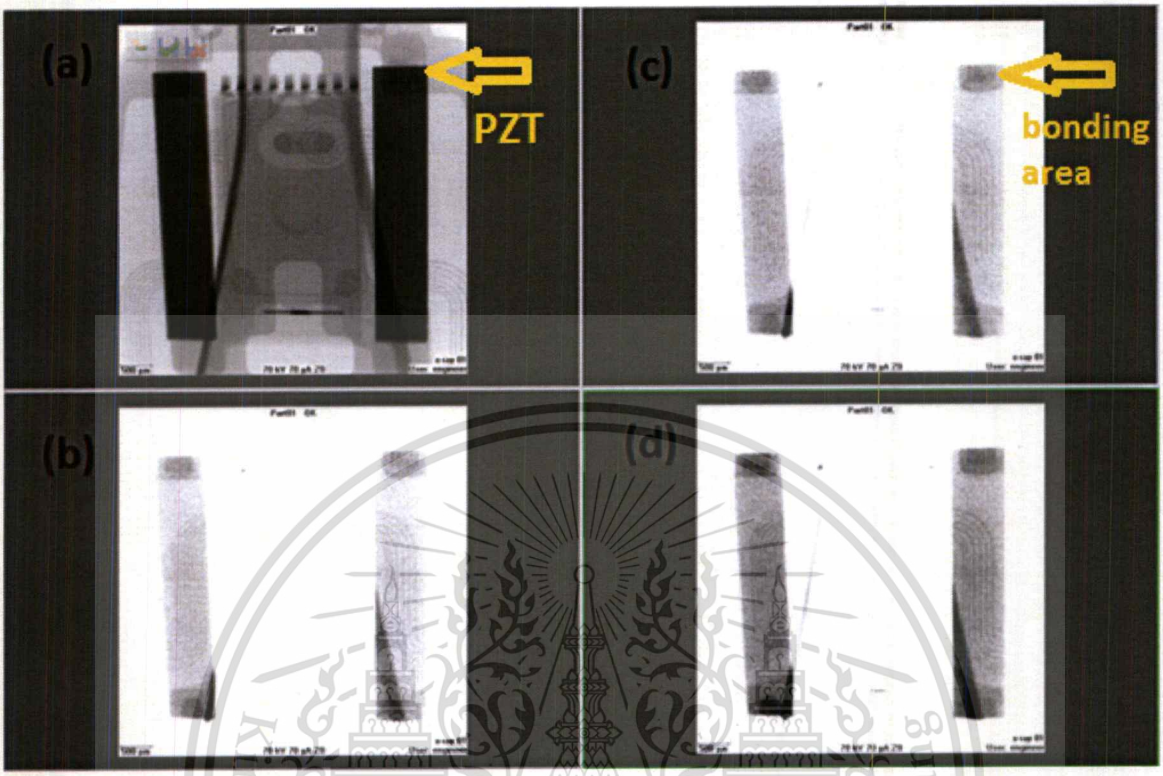

Figure 5.1 X-Ray image of piezoelectric
(a) and (b) good parts, (c) and (d) failed parts

The Fig. 5.1 (a) and (b) shows X-Ray images of the good parts and (c) and (d) for the failed parts. In (a) shows the piezoelectric location placed on suspension. (b), (c) and (d) shows the adhesive bonding area underneath the piezoelectric. The images between good parts and the stroke failure parts are comparable. No adhesive void or mechanical damages found at all joint areas.

5.1.2 SEM Inspection and Shear Test

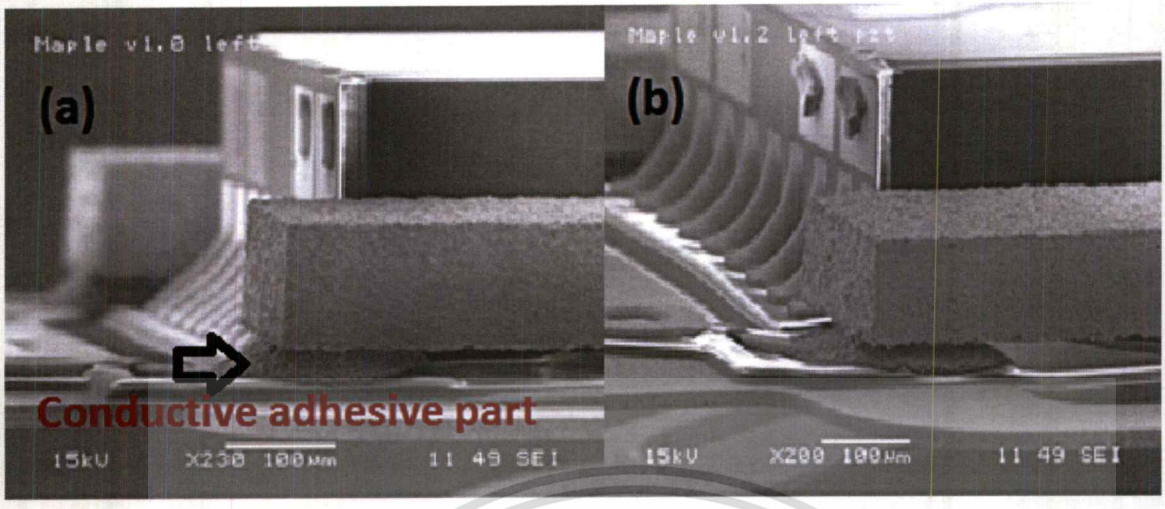

Figure 5.2 SEM image at side of piezoelectric
(a) good and (b) failed part

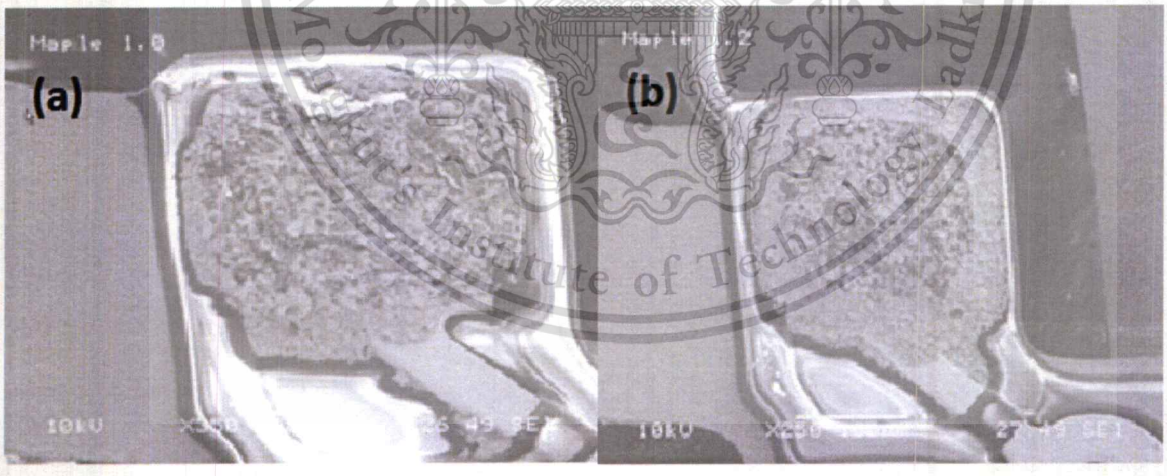

Figure 5.3 SEM image of bonded surface on suspension after shear test
(a) good and (b) failed part

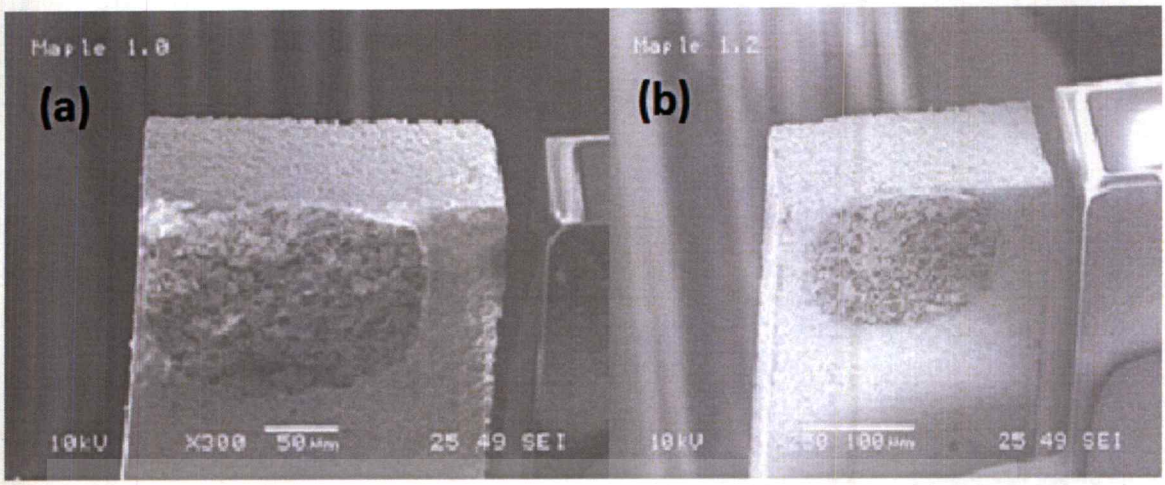

Figure 5.4 SEM image of bonded surface on PZT after shear test (a) good and (b) failed part

The SEM images at side of piezoelectric between good parts and the stroke failure parts are comparable. No mechanical damages found at all joint areas and also surface both sides of piezoelectric are in good condition see in the Fig. 5.2. Moreover after shear test at bonded area, there are no any abnormal structure found on both suspension joint and piezoelectric joint area. The adhesive joints area were in good shape as seen in Fig. 5.3 and 5.4 respectively.

5.2 Electrical Properties Characterization

In order to be able to determine the source of stressor, the HGA Process mapping and verification by each step of the head gimbal assembly is the key this research. The capacitance and resistance measurement has been performed at incoming parts (Raw suspension) using multi-meter. It has been previously explained in Chapter 3 that

when a voltage is applied cross a capacitor made of normal dielectric material, a charge result on the plates or electrodes of the capacitor. Charge can also be produced on the electrodes of a capacitor made of a piezoelectric material by the application of stress. This is known as the Direct Piezoelectric Effect. Conversely, the application of a field to the material will result in strain. This is know as the Inverse Piezoelectric Effect. So, the multi-meter is considered as tool to measure capacitance and resistance in HGA manufacturing process mapping as previously explained more details in Chapter 2.

The result shows both capacitance and resistance values are acceptable with an average of capacitance 373.80pF and the average of resistance 400.25Ω respectively as showed in Fig. 5.5 (a) for capacitance and (b) for resistance. The standard deviation of capacitance and resistance of an incoming parts is 13.56 and resistance 74.90 respectively. Statistical distribution for both capacitance and resistance as showed in Fig. 5.5 (a) and (b). The statistical distribution is created by using Minitab software.

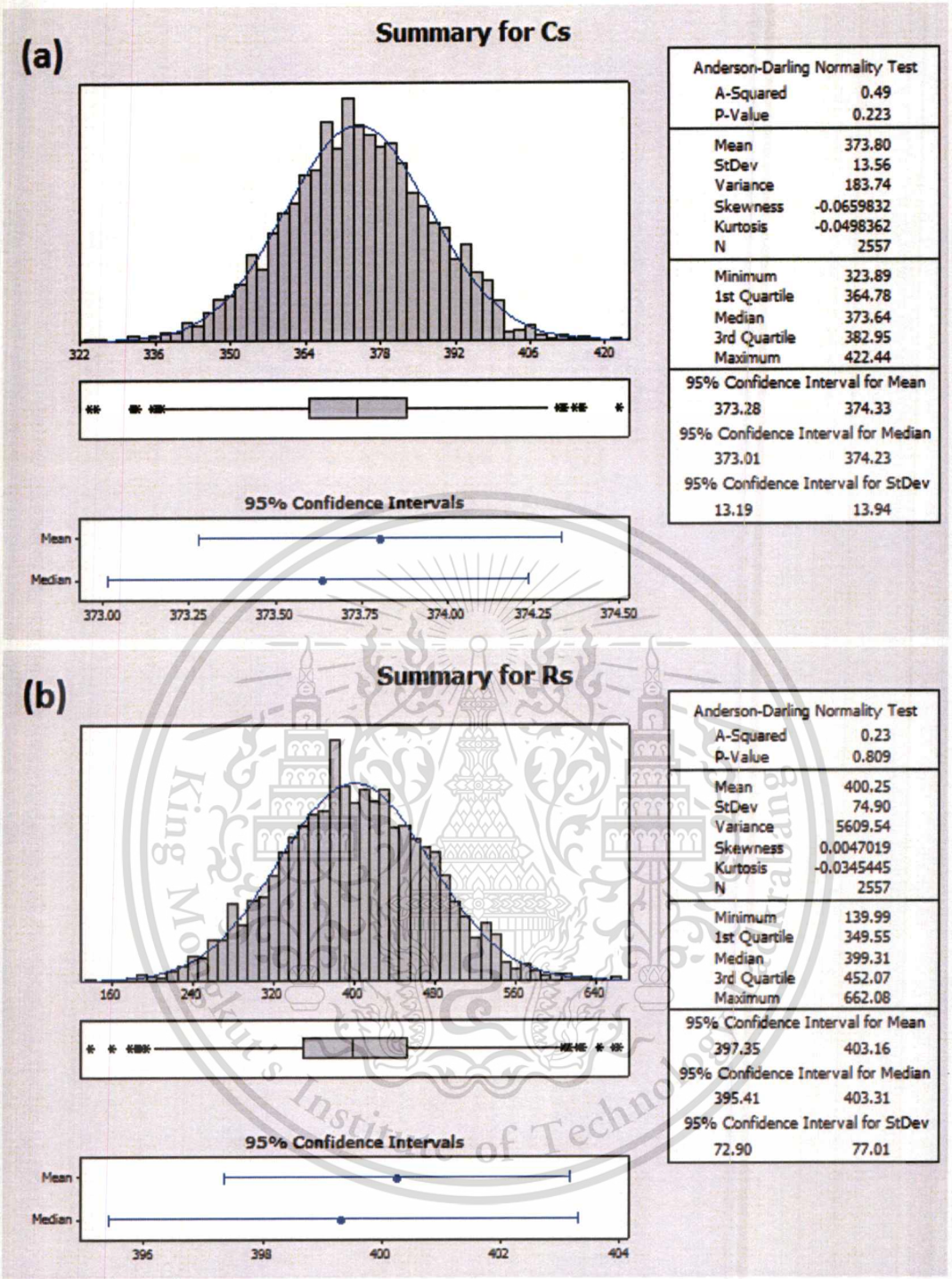

Figure 5.5 (a) Capacitance and (b) Resistance measurement of piezoelectric at incoming parts (suspension level)

The capacitance and resistance measurement has been performed from all stroke failure parts from electrical tester using multi meter and the results show both capacitance and resistance rejected with an average value of 245.59pF (both tabs) and 211Ω respectively. The standard deviation of capacitance and resistance of stroke failure parts is 5.94 and resistance 27.20. Statistical distribution for both capacitance and resistance (both tabs) as shown in Fig. 5.6-5.7. It was confirmed for true failure.

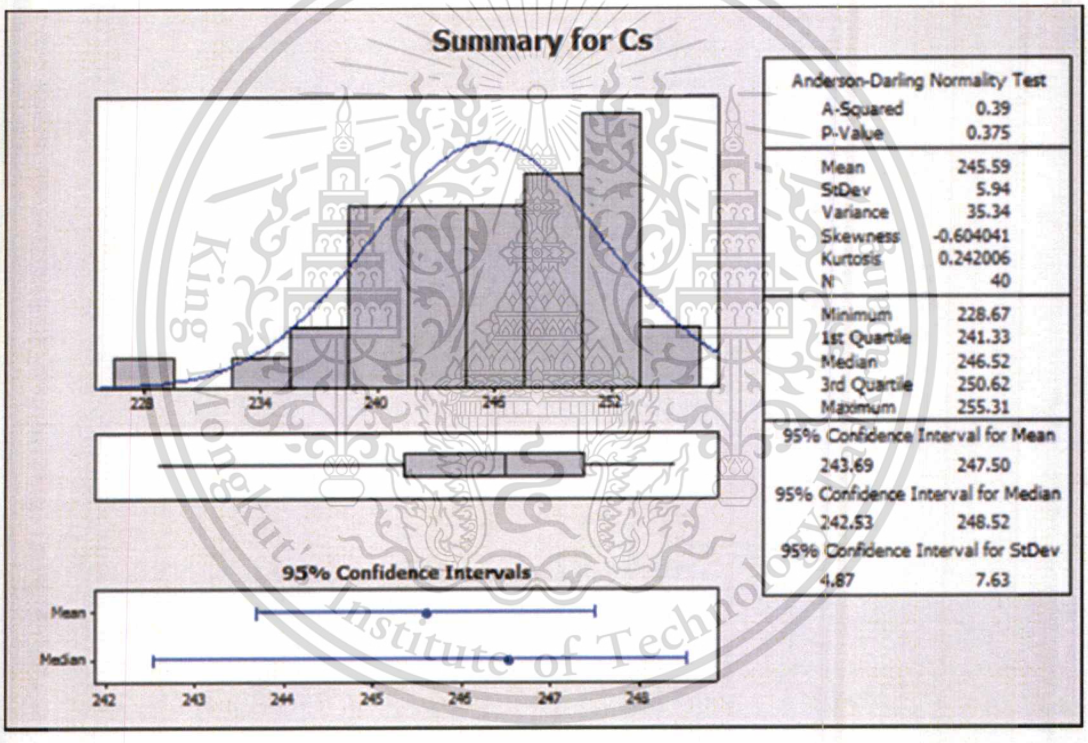

Figure 5.6 Capacitance measurement of piezoelectric for stroke failure parts

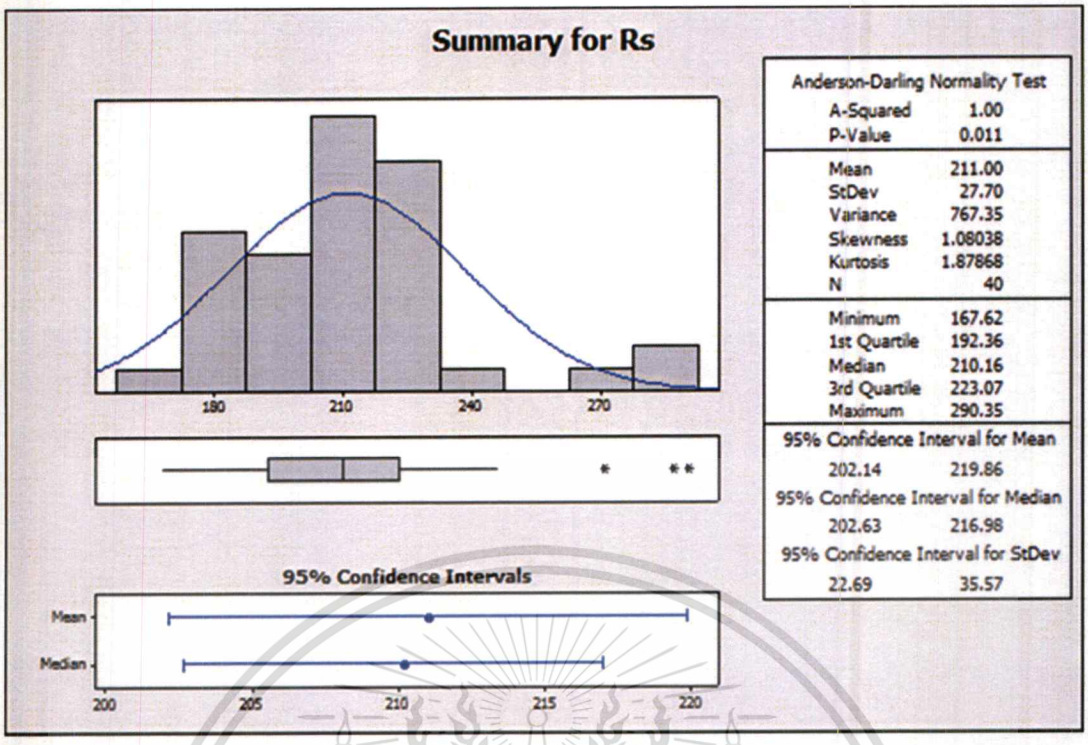

Figure 5.7 Resistance measurement of piezoelectric for stroke failure parts

The capacitance for macro head gimbal process mapping has been performed by using multi-meter in the head gimbal assembly process and the evaluation result. The average of capacitance measurement at incoming parts is 427pF, at head gimbal assembly operations is 292pF and after electrical test is 281pF. The capacitance dropped in approximately 30% from incoming as shown in Table 5.1

No.	TGA Level (nF)	HGA Level (nF)	HGAs After ET (nF)
1	0.418	0.3	0.306
2	0.417	0.28	0.283
3	0.415	0.297	0.172
4	0.427	0.285	0.285
5	0.418	0.287	0.285
6	0.426	0.298	0.286
7	0.532	0.292	0.289
8	0.418	0.299	0.289
9	0.423	0.296	0.288
10	0.413	0.291	0.288
11	0.405	0.289	0.285
12	0.426	0.291	0.286
13	0.428	0.297	0.289
14	0.427	0.295	0.29
15	0.413	0.287	0.287
Average	0.427	0.292	0.281
	% Cs Drop	31.56	34.31

Table 5.1 Macro Process capacitance line mapping

The capacitance for micro head gimbal process mapping has been performed using multi-meter. From the evaluation result, the average of capacitance measurement at incoming parts is 630pF, at suspension load station is 630pF, at slider attach station is 700pF, at IR Oven station is 460pF and at Thermal Interconnect station is 460pF. Therefor, the

capacitance dropped in approximately 30% from incoming as shown in Fig. 5.8

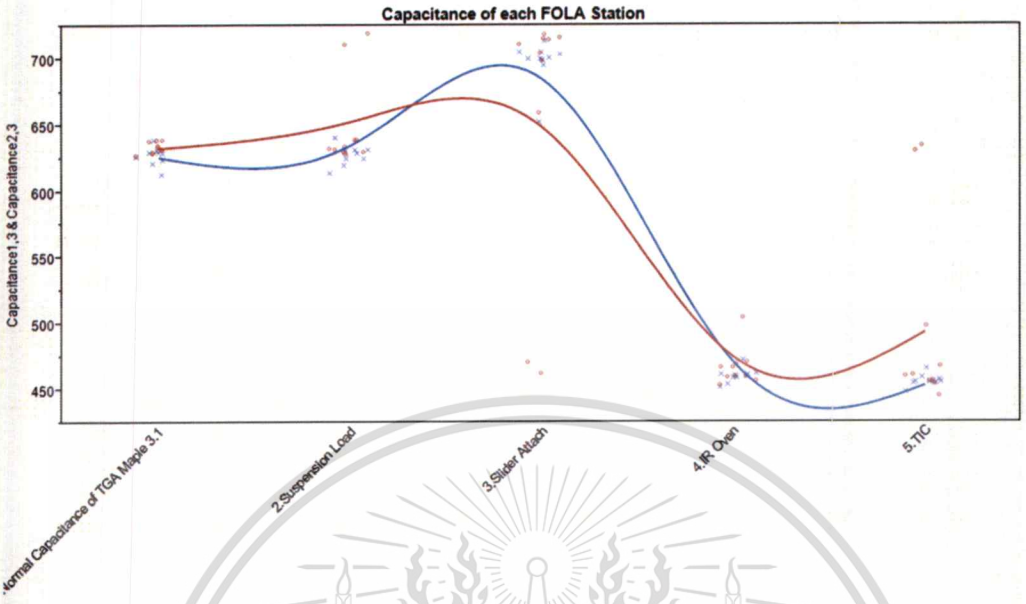

Figure 5.8 Micro Process capacitance line mapping

5.3 Sources of stroke failure inside the infrared oven cure

This experiment is to study and find sources of stroke failure inside the infrared oven cure station. The infrared oven is set and controlled for 10 parts per carrier. The infrared source is placed underneath parts and radiate close to gimbal bond area. There are 4 groups of Infrared Energy Level to be evaluated at 1.51, 2.51, 3.62 and 4.33 J/cm^2 and the current energy level at 3.14 J/cm^2. Sampling 50 TGAs at incoming suspension and use multi meter to measure capacitance for all TGAs and split into 5 groups.

Temperature absorption calculated from regression equation below. This temperature absorption regression equation below is from

Seagate Design team in the US. The design team was conducted and concluded for this regression equation for this suspension design and recommended to apply in this research experimental.

Temperature VS IR Energy Regression

$$\left(Temperature\ (degree\ C) = 35.77 + 22.16\ IR\ Energy\ \left(\frac{J}{cm2}\right)\right)$$

The Infrared energy level has been studied to be able to control heat transfer to the piezoelectric on suspension using temperature regression equation above. There are 5 groups of an infrared energy level have been conducted and studied. The first group is to set an infrared energy level as normal production build at 3.14 J/cm^2. The mean of capacitance measurement at TGA level (incoming suspension) is 266pF, at HGA level (after IR Oven machine) is 277pF and after electrical test is 258pF. The percentage of capacitance between incoming suspension to compare with HGA process after IR Oven shows no drop. However, the capacitance comparison between incoming suspension and HGA process after electrical test is 4.39% as shown in Table 5.2.

Normal Group

IR Energy = 3.14 J/cm²

Estimate temperature = 105.35 degree celsius

No	Capacitance Value (nF)		
	TGA Level	HGA Level 1 (After IR Oven)	HGA Level 2 (After ET)
1	0.267	0.272	0.257
2	0.266	0.282	0.257
3	0.265	0.279	0.256
4	0.266	0.278	0.256
5	0.268	0.280	0.257
6	0.267	0.279	0.257
7	0.266	0.277	0.257
8	0.267	0.279	0.256
9	0.263	0.273	0.264
10	0.265	0.278	0.263
Avg.	0.266	0.2777	0.258
	% Cs Drop	No Cs drop	4.39

Table 5.2 Capacitance reading for normal group at Infrared energy level at 3.14 J/cm^2

The second group is to set an infrared energy level at 1.51 J/cm^2. The mean of capacitance measurement at TGA level (incoming suspension) is 265pF, at HGA level (after IR Oven machine) is 286pF and after electrical test is 267pF. The percentage of capacitance between incoming suspension to compare with HGA process after IR Oven and after electrical test shows no drop as shown in Table 5.3.

1) IR Energy = 1.51 J/cm²

Estimate temperature = 69.23 degree celsius

No	Capacitance Value (nF)		
	TGA Level	HGA Level 1 (After IR Oven)	HGA Level 2 (After ET)
1	0.261	0.283	0.264
2	0.265	0.284	0.265
3	0.267	0.288	0.269
4	0.266	0.287	0.268
5	0.265	0.287	0.267
6	0.265	0.288	0.268
7	0.265	0.286	0.268
8	0.266	0.287	0.268
9	0.265	0.287	0.269
10	0.265	0.285	0.269
Avg.	0.265	0.2862	0.2675
	% Cs Drop	No Cs drop	No Cs Drop

Table 5.3 Capacitance reading at Infrared energy level at 1.51 J/cm^2

The third group is to set an infrared energy level at 2.51 J/cm^2. The mean of capacitance measurement at TGA level (incoming suspension) is 268pF, at HGA level (after IR Oven machine) is 291pF and after electrical test is 275pF. The percentage of capacitance between incoming suspension to compare with HGA process after IR Oven and after electrical test shows no drop as shown in Table 5.4.

2) IR Energy = 2.51 J/cm²

Estimate temperature = 91.40 degree celsius

No	Capacitance Value (nF)		
	TGA Level	HGA Level 1 (After IR Oven)	HGA Level 2 (After ET)
1	0.263	0.285	0.273
2	0.267	0.289	0.274
3	0.265	0.289	0.274
4	0.269	0.287	0.275
5	0.266	0.290	0.274
6	0.269	0.290	0.275
7	0.270	0.292	0.274
8	0.267	0.295	0.278
9	0.273	0.296	0.279
10	0.270	0.295	0.276
Avg.	0.268	0.291	0.275
	% Cs Drop	No Cs drop	No Cs Drop

Table 5.4 Capacitance reading at Infrared energy level at 2.51 J/cm^2

The fourth group is to set an infrared energy level at 3.62 J/cm^2. The mean of capacitance measurement at TGA level (incoming suspension) is 273pF, at HGA level (after IR Oven machine) is 257pF and after electrical test is 235pF. The percentage of capacitance comparison between incoming suspension and HGA process after IR Oven is 5.9%. Also the percentage of capacitance comparison between incoming suspension and HGA process after electrical test is 13.88% as shown in Table 5.5.

3) IR Energy = 3.62 J/cm²

Estimate temperature = 116 degree celsius

No	Capacitance Value (nF)		
	TGA Level	HGA Level 1 (After IR Oven)	HGA Level 2 (After ET)
1	0.269	0.243	0.223
2	0.289	0.274	0.251
3	0.270	0.252	0.231
4	0.268	0.254	0.232
5	0.291	0.275	0.251
6	0.270	0.256	0.232
7	0.270	0.255	0.230
8	0.269	0.253	0.229
9	0.267	0.254	0.236
10	0.268	0.254	0.237
Avg.	0.273	0.257	0.235
	% Cs Drop	5.9	13.88

Table 5.5 Capacitance reading at Infrared energy level at 3.62 J/cm^2

The fifth group is to set an infrared energy level at 4.33 J/cm^2. The mean of capacitance measurement at TGA level (incoming suspension) is 276pF, at HGA level (after IR Oven machine) is 212pF and after electrical test is 195pF. The percentage of capacitance comparison between incoming suspension and HGA process after IR Oven is 23.22%. Also the percentage of capacitance comparison between incoming suspension and HGA process after electrical test is 29.41% as shown in Table 5.6.

4) IR Energy = 4.33 J/cm²

Estimate temperature = 131.72 degree celsius

No	Capacitance Value (nF)		
	TGA Level	HGA Level 1 (After IR Oven)	HGA Level 2 (After ET)
1	0.263	0.203	0.184
2	0.291	0.219	0.206
3	0.270	0.209	0.189
4	0.272	0.201	0.191
5	0.272	0.202	0.191
6	0.293	0.226	0.207
7	0.289	0.227	0.205
8	0.270	0.210	0.193
9	0.271	0.212	0.192
10	0.270	0.211	0.191
Avg.	0.276	0.212	0.195
	% Cs Drop	23.22	29.41

Table 5.6 Capacitance reading at Infrared energy level at 4.33 J/cm^2

Further study on the relationship between an infrared energy level and electrical stroke reading more data point have been collected in the range of an infrared energy level from 2.5 to 3.5 J/cm^2 as shown in Fig. 5.9. The infrared energy level less than 3.1 J/cm^2 is no risk for stroke failure at electrical tester station, the infrared energy level between 3.1 to 3.3 J/cm^2 is at risk for stroke failure at electrical tester station and if the infrared energy level more than 3.3 J/cm^2 is dead at electrical tester station. Based on temperature absorption calculation with an infrared energy level at 3.62 J/cm^2 is equal to 116 degree Celsius which over than half of curie temperature of piezoelectric material. Piezoelectric ceramics suffer from loss of polarization as dipoles have a tendency to revert back to random orientation at high temperature; this loss of polarization is called thermal degradation. The thermal degradation is associated with an external influence and usually implies a large

detrimental change to a property of a material. In order to minimize the thermal degradation, maximum application of piezoelectric material is generally restricted to half of curie temperature.

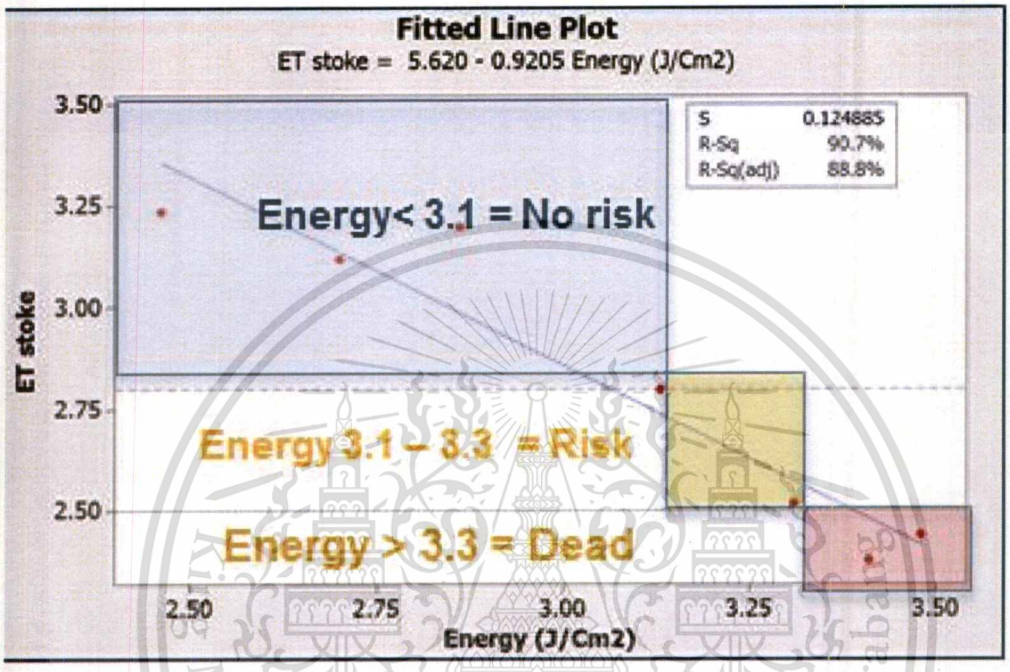

Figure 5.9 Infrared energy level optimization

5.4 Re-poling Piezoelectric Verification

This experiment is to study whether re-poling the stroke failure parts by applying a large electrical voltage at 92.5 volts will recover the alignment of ferroelectric diploes back to the original direction or not. The electrical voltage value of 92.5 volts was recommended from Seagate Suspension Design in the US team. The design team was conducted and concluded this voltage value from the US design site.

The experiment results, the stroke failure parts have been confirmed by measuring capacitance both sides of piezoelectric on suspension with reading between 120 to 133 pF for the left piezoelectric and reading between 112 to 120 pF for the right piezoelectric. Also combined the capacitance for both sides of piezoelectric with the capacitance reading in a range between 246 to 252 pF. Then, applying a large electrical voltage at 92.5 volts for re-poling piezoelectric material and measure the capacitance both sides of piezoelectric with reading between 150 to 160 pF for the left piezoelectric and 155 to 165 pF for the right piezoelectric respectively. Also combined the capacitance for both sides of piezoelectric with the capacitance reading in a range between 377 to 381 pF as shown in table 5.7.

	Capacitance (pF)					
	Stroke Failure			After re-poling PZT		
	Left PZT	Right PZT	Both PZT	Left PZT	Right PZT	Both PZT
Part 1	120.9	120.9	246	158.9	163.7	377
Part 2	132	118.3	247	154.1	164.3	379
Part 3	133.3	116.1	251	149.7	158.6	380
Part 4	132.4	112.1	252	160	154.7	381

Table 5.7 Capacitance measurement after re-poling PZT

Another tool is used to verify mechanical stroke measurement by using the wave C. The stroke failure parts haven been measured at wave C and the normalized stroke reading between -77.35 to -95.72 nm/volt. Then, apply a large electrical voltage at 92.5 volts to re-poling piezoelectric material on suspension and measure stroke reading of

those stroke failure parts, the normalized stroke reading between -85.53 to -86.55 nm/volt as shown in table 5.8.

	Stroke Failure (nm/V)	After re-poling PZT (nm/V)
Part 1	-95.72	-86.55
Part 2	-77.35	-85.53
Part 3	-88.56	-86.33
Part 4	-91.03	-86.41
Part 5	-94.58	-86.48

Table 5.8 Mechanical normalized stroke measurement after re-poling PZT by using wave C

Cross section and SEM inspection result showed comparable between good parts and stroke failure parts after re-poling. There is no structure changed and damaged at all layers as shown in Fig. 5.10 – 5.11.

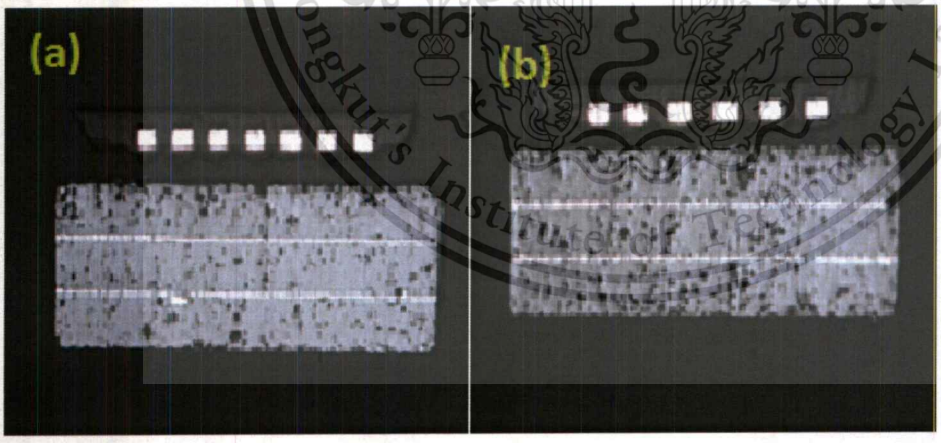

Figure 5.10 SEM images good parts after cross section (a) left and (b) right

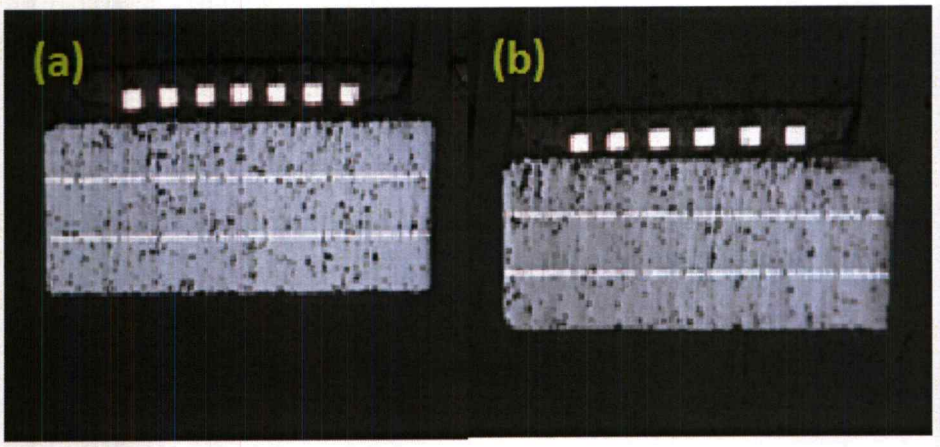

Figure 5.11 SEM images rejected parts after re-poling and cross section

(a) left and (b) right

CHAPTER 6
Conclusions

6.1 Structure Characterization

The X-Ray images between good parts and stroke failure parts have been verified for any mechanical damage to the piezoelectric on suspension. The result showed no mechanical damages found at all joint areas.

The SEM images between good parts and stroke failure parts with high magnification inspection have been verified for any mechanical damage on the piezoelectric structure. There are no mechanical damage and also surface both sides of piezoelectric are in good condition. Moreover after shear test at bonded area, there are no any abnormal structure found on both suspension joints and piezoelectric joint areas. The adhesive joint area was in good shape as seen in section 5.3 and 5.4 respectively.

6.2 Electrical Properties Characterization

In order to be able to determine the source of stressor, the HGA Process mapping and verification by each step of the head gimbal assembly is the key of this research. The capacitance and resistance measurement has been performed at incoming parts (Raw suspension) using multi-meter.

The result shows both capacitance and resistance values are acceptable with an average of capacitance 373.80pF and the average of resistance 400.25Ω respectively. The standard deviation of capacitance of incoming parts is around 13.56 and resistance is around 74.90 respectively. The result shows no issue found at incoming suspension.

The capacitance line mapping has been performed using multi-meter in the head gimbal assembly process steps both macro and micro process. From the evaluation result, the average of capacitance measurement at incoming parts is 630pF, at suspension load station is 630pF, at slider attach station is 700pF, at IR Oven station is 460pF and at Thermal Interconnect station is 460pF. The result shows no issue found at incoming suspension only in the head gimbal assembly process at an infrared (IR) oven cure machine can cause the capacitance dropped in approximately 30% from incoming suspension from vendor (from micro process mapping).

6.3 Source of Stroke Failure inside the Infrared Oven

The Infrared energy has been studied and optimized to be able to control heat transfer to the piezoelectric on suspension by using temperature regression equation as indicated in section 5.3. There are 4 groups of Infrared Energy Level to be evaluated at 1.51, 2.51, 3.62 and 4.33 J/cm^2 and the current energy level at 3.14 J/cm^2. Sampling 50 TGAs at incoming suspension and use multi meter to measure capacitance for all TGAs and split into 5 groups.

The first group is to set an infrared energy level as normal production build at 3.14 J/cm^2. The mean of capacitance measurement at TGA level (incoming suspension) is 266pF, at HGA level (after IR Oven machine) is 277pF and after electrical test is 258pF. The percentage of capacitance between incoming suspension to compare with HGA process after IR Oven shows no drop. However, the capacitance comparison between incoming suspension and HGA process after electrical test is 4.39%. It means that the stroke failure come from this infrared energy set up which required lower infrared energy and perform an optimization.

The second group is to set an infrared energy level at 1.51 J/cm^2. The mean of capacitance measurement at TGA level (incoming suspension) is 265pF, at HGA level (after IR Oven machine) is 286pF and after electrical test is 267pF. The percentage of capacitance between incoming suspension to compare with HGA process after IR Oven and after electrical test shows no drop. It means that this infrared energy level is safe for stroke test.

The third group is to set an infrared energy level at 2.51 J/cm^2. The mean of capacitance measurement at TGA level (incoming suspension) is 268pF, at HGA level (after IR Oven machine) is 291pF and after electrical test is 275pF. The percentage of capacitance between incoming suspension to compare with HGA process after IR Oven and after electrical test shows no drop. It means that this infrared energy level is safe for stroke test.

The fourth group is to set an infrared energy level at 3.62 J/cm^2. The mean of capacitance measurement at TGA level (incoming suspension) is 273pF, at HGA level (after IR Oven machine) is 257pF and after electrical test is 235pF. The percentage of capacitance comparison between incoming suspension and HGA process after IR Oven is 5.9%. Also the percentage of capacitance comparison between incoming suspension and HGA process after electrical test is 13.88%. It means that this infrared energy level is at risk for stroke failure.

The fifth group is to set an infrared energy level at 4.33 J/cm^2. The mean of capacitance measurement at TGA level (incoming suspension) is 276pF, at HGA level (after IR Oven machine) is 212pF and after electrical test is 195pF. The percentage of capacitance comparison between incoming suspension and HGA process after IR Oven is 23.22%. Also the percentage of capacitance comparison between incoming suspension and HGA process after electrical test is 29.41%. It means that at this infrared energy level is the cause of stroke failure and parts will dead.

From an infrared energy experimental result, it indicates that the piezoelectric has been degraded at an infrared oven machine from heat transfer which is transfer more than half of curies temperature of piezoelectric material.

From the relationship between an infrared energy level and electrical stroke reading more data point have been collected in the range of an infrared energy level from 2.5 to 3.5 J/cm^2. And the result showed the infrared energy level less than 3.1 J/cm^2 is no risk for stroke

failure at electrical test station, the infrared energy level between 3.1 to 3.3 J/cm^2 is at risk for stroke failure at electrical test station and if the infrared energy level more than 3.3 J/cm^2 is dead at electrical test station. Based on temperature absorption calculation with an infrared energy level at 3.62 J/cm^2 is equal to 116 degree Celsius which over than half of curie temperature of piezoelectric material. Piezoelectric ceramics suffer from loss of polarization as dipoles have a tendency to revert back to random orientation at high temperature; this loss of polarization is called thermal degradation. The thermal degradation is associated with an external influence and usually implies a large detrimental change to a property of a material. In order to minimize the thermal degradation, maximum application of piezoelectric material is generally restricted to half of curie temperature

In conclusion, the safe zone for infrared energy level without any stroke failure between 2.7 to 3.1 J/cm^2 due to if an energy level lower than 2.7 J/cm^2. The IR oven will not properly cure and causing slider pop out of gimbal area per the previous design study.

6.4 Re-poling Piezoelectric Verification

The stroke failure has been confirmed by applying a large voltage at 92.5 volt for re-poling the piezoelectric and measure capacitance and stroke. The experiment results, the stroke failure parts have been confirmed by measuring capacitance both sides of piezoelectric on suspension with reading between 120 to 133 pF for the left piezoelectric and reading between 112 to 120 pF for the right piezoelectric. Also

combined the capacitance for both sides of piezoelectric with the capacitance reading in a range between 246 to 252 pF. Then, applying a large electrical voltage at 92.5 volts for re-poling piezoelectric material and measure the capacitance both sides of piezoelectric with reading between 150 to 160 pF for the left piezoelectric and 155 to 165 pF for the right piezoelectric respectively. Also combined the capacitance for both sides of piezoelectric with the capacitance reading in a range between 377 to 381 pF. It means after re-poling piezoelectric the capacitance and the normalized stroke reading are back to normal with acceptable in an operating range (377 to 381 pF). The cross section and SEM images result both good parts and stroke failure parts after re-poling are comparable. There is no structural changed and damaged at all layers.

The stroke failure parts haven been measured at wave C for mechanical stroke verification and the normalized stroke reading between -77.35 to -95.72 nm/volt. Then, apply a large electrical voltage at 92.5 volts to re-poling piezoelectric material on suspension and measure stroke reading of those stroke failure parts, the normalized stroke reading between -85.53 to -86.55 nm/volt. It means that after re-poling piezoelectric material the capacitance and the normalized stroke reading back to normal with an acceptable operating range at -85 nm/Volt.

In conclusion, the structure characterization results show no mechanical damage related issue by using X-Ray and SEM inspection technique. Also an incoming suspension has no issue. The capacitance

line mapping found that the Infrared Oven Cure machine is cause of problem. The Infrared energy optimization has been studied and showed that energy higher than 3.1 J/cm^2 can cause piezoelectric on suspension to degrade or dead from heat transfer per temperature regression equation. Once the temperature increases over half of curie's temperature, piezoelectric material starts to degrade. The optimum infrared energy level must be controlled between 2.7 to 3.1 J/cm^2 due to if the energy level lower than 2.7 J/cm^2. The IR oven will not properly cure and causing slider pop out of gimbal area per the previous design study.

It is worth to note that in this research there are some constrains in the experiment set up. Firstly, the IR oven used in this experiment is used as normal production line. Therefore the experiment could be conducted only when the IR oven was idle. As a result, the experiments might not be carried out continuously at the same period of time. Secondly, the cost of new suspension design is high and only few parts. The new design always rapidly change. Consequently, the suspension design could be changed and can not get the same design parts to be carried out continuously at the same period of time. Thus at the different suspension design may have some effects on the evaluation results.

6.5 Recommendations and Further Work

This research is mainly to identify the stressor in HGA manufacturing process and did not try to change the PZT material and

also the optimum re-poling level of the stroke failure parts. To understand suspension design and ferroelectric dipole moment recovery are determine as

1) Get the new PZT material to verify whether new material more robustness than the existing PZT material structure
2) The optimum re-poling level of the stroke failure parts more understanding for ferroelectric dipole moment by reversing the poling voltage and increasing the temperature beyond the materials Currie point. Also the cross section with SEM images may not high magnification and resolution enough to classify and differentiate piezoelectric material structure before re-poling and after re-poling.

REFERENCE

[1] B. Jeff, W. R. Cook, JR. and H. Jaffe, "Piezoelectric Ceramics," *Academic Press: London, New York, (1971)*

[2] Hideki Kuwajima, Hirokazu Uchiyama, Yuko Ogawa, Hiroyuki Kita, and Kaoru Matsuoka, "Manufacturing Process of Piezoelectric Thin-Flim Dual-Stage Actuator and Its Reliability for HDD", *IEEE Transactions on Magnetics, Vol. 38, No 5, September 2002*

[3] Mark D. Bedillion, Mahmut Karaman, and Patrick B. Chu Members, IEEE, "Spinstand Control Characterization of an Electromagnetic Slider Microactuator", *American Control Conference, June 8-10, 2005, Portland, OR, USA*

[4] Kwong Wah Chan, and Wei-Hsin Liao Smart Materials and Structures Laboratory, Department of Automation and Computer-Aided Engineering, The Chinese University of Hongkong, "Precision Positioning of Hard Disk Drives Using Piezoelectric Actuators with Passive Damping", *Proceeding of the 2006 IEEE, International Conference on Mechatronics and Automation, June 25 – 28, 2006, Luoyang, China*

[5] K. Mori, T. Muneomoto, H. Otsuki, Y. Yamaguchi and K. Akagi "A dual-stage magnetic disk drive actuator using a piezoelectric device for a high track density", *IEEE TRANSECTIONS ON MAGNETICS, VOL. 27, NO. 6, November 1991*

[6] Kenn Oldhamm, Sarah Fliex, Richard Convey and Roberto Horowitz, "Design and Control of a Dual-Stage Disk Drive Servo System with a

high-aspect ratio Electrostatic Microactuator", *American Control Conference, June 11-13,2008*

[7] Antonie Ledoux, "Theory of Piezoelectric Materials and Theirs Applications in Cilvil Engineering", *MIT Jun 2011*

[8] Jame R. Phillips, "Piezoelectric Technology Primer", Albuquerque, New Mexico 87113

[9] C. Sawer, and C. Tower, "Rochelle salt as a dielectric ceramics," *Physical Review, 35, (1930)*

[10] G. H. Hartling, "Ferroelectric ceramics: History and technology," *Journal of American Ceramic Society, 82, (1992)*

[11] N. Izyumskaya, Y. I. Alivov, S. J. Cho, H. Morkc, H. Lee, and Y. S. Kang, "Processing, structure, properties and applications of PZT thin films," *Critical Reviews in Solid State and Materials Science, 32, (2007)*

[12] D. Berlincourt, "Piezoelectric ceramic compositional development," *Journal Acoustic Society of America, 91, (1992)*

[13] C. A. Randall, N. Kim, J. P. Kucera, W, Cao, and T. R. Shrout, "Intrinsic and extrinsic size effect in fine grained morphotropic phase boundary lead zirconate titanate ceramics," *Journal of American ceramic society, 81, (1998)*

[14] D. Damjanovic, "Ferroelectric, dielelctric and piezoelectric properties of ferroelectric thin films and ceramics," *Prog Phys, 61, (1998)*

[15] B. Guiffard, E. Boucher, L. Lebrun, and D. Guyomar, Characteristics of F doped PZT ceramics using different fluorine sources," *Material Science and Engineering, 137, (2007)*

[16] B. Jaffe, W. R. Roth, and Marzullo, "Piezoelectric properties of lead zirconate – lead titanate solid-solution ceramics," *Journal of Applied Physics, 25, (1954)*

[17] T. R. Shrout, and S. J. Zhang, "Lead free piezoelectric ceramics: Alternatives for PZT?." *Journal of Electroceramic, 19, (2007)*

[18] B. Noheda, and J. A. Gonzalo, "Tetragonal-to-monoclinic phase transition in ferroelectric perovskite : The structure of PbZr0.52Ti0.48O3," *Physical Review, 61, (2000)*

[19] B. Noheda, "Structure and high piezoelectricity in lead oxide solutions," *Current Opinion in Solid State and Materials, 6, (2002)*

[20] S. B. Herner, "The use of acceptor dopants to lower the loss tangent in barium strontium titanate," *Thesis: Pennsylvania State University, (1993)*

[21] Measurement of Properties of Piezoelectric Ceramics, Sensor Technology Limited, BM91-309, *Manufacturer Handbook, (1991)*

[22] A. J. Moulson and J. M. Herbert, "Electroceramics: Materials, properties, applications, *Chapman and Hall: London, New York, (1992)*

[23] Q. F. Zhou, H. L. W. Chan, and L. Choy, Nanocrystalline Powder and Fibres of Lead Zieconate Titanate Prepared by the Sol-Gel Process, *Journal of Materials Processing Technology, 63, No 1-3 (1997), pp. 281-285*

[24] Z. Ounaies, Sol-Gel and Microwave Processing of PZT Materials for Sensor and Actuator Applications, *the Pennsylvania State University, 1995*

[25] J. P. Whitman, Hydrothermal Preparation and Fabrication of Lead Zirconate Titanate (PZT) Ceramics, *the Pennsylvania State University, 1993*

[26] C. Near, G. Shmidt, K. McNeal and R. Gentilman, "Injection Molded PZT Actuators, *SPIE 5th Annual Symposium on Smart Structures and Materials Proceedings, 3326 (1998), pp. 323-331*

[27] L. M. Levinson, "Electronic Ceramics : Properties, Devices, and Applications, *General Electric Company: New York, (1998)*

[28] ACX Controls Expert, www.ACX.com

[29] R. E. Eitel, C. A. Randall, T. R. Shrout, and S. E. Park, "Praparation and characterization of high temperature perovskite ferroelectrics in the solid solution (1-X)BiScO3-(X)PbTiO3," *Japanese Journal of Applied Physics, 41, (2002)*

[30] S. Chen, X. Dong, C. Mao, and F. Cao, "Thermal stability of (1-X)BiScO3-xPbTiO3 piezoelectric ceramics for high temperature sensor applications," *Journal of American Ceramic Society, 89, (2006)*

[31] T.L. Jordan, and Z. Ounaies, "Piezoelectric Ceramics Characterization" *ICASE Report No. 201-28, Sep 2001*

Suspension with Piezoelectric Effects on High Temperature in HGA Manufacturing Process

Hussadin Thungsakul[#1]
College of Data Storage Technology and Applications
King Mongkut's Institute of Technology Ladkrabang
BKK, Thailand, 10520
[1]Hussadint92@gmail.com

Wanchai Pijitrojana[#2]
[#]*Department of Electrical and Computer Engineering*
Thammasat University, Klong Luang
Pratumthani, Thailand, 12120
[2]pwanchai@engr.tu.ac.th

Winadda Wongwiriyapan[#3]
[#]*College of Nanotechnology*
King Mongkut's Institute of Technology Ladkrabang
BKK, Thailand, 10520
[3]kwwinadd@kmitl.ac.th

***Abstract*— The Suspension with piezoelectric has been considered as the most promising candidate for nano positioning with very high accuracy for Hard Disk Drive with high areal density product. In Head Gimbal Assembly (HGA) manufacturing process there are many steps causing stress and effect on depolarization of poled lead titanate zirconate (PZT) ceramics that contribute to head performance called "Stroke" test at electrical tester. Failure analysis and process mapping were conducted to identify which process steps can contribute to Stroke failure at electrical tester. Capacitance measurement technique is used to determine which process can cause Stroke failure and need to investigate and optimize for hard disk drive process control. It is found that the capacitance has changed after Infrared (IR) oven cure process once increasing temperature to 50% of curie temperature (*Tc*) of the piezoelectric material attached on the suspension.**

Keywords- Temperature-effect piezoelectric, Depolarization of ferroelectric ceramics, Thermal Degradation

I. INTRODUCTION

As the areal density of hard disk drive recording systems increases beyond 750Gb/in^2, more process and performance constraints should be considered for keeping up with the shrinking size of the heads. On the other hand, piezoelectric material, continues to dominate and commonly used for nano positioning and high accuracy for piezoelectric actuators applications in Hard Disk Drive (HDD) manufacturing process. Primary designs for all those technology demonstrations as well as commercial products are based on the lead titanate zircronate (PZT).[1] The conversion of mechanical energy in a piezoelectric material into electrical energy and reverse effect is the basis for sensors and actuators. Piezoelectric materials have numerous applications like ultra high temperature accelerometers, pressure, transducers, acoustic emission, ultrasonic cleaning, welding, high voltage generators, medical therapy etc.[2]

Discovery of piezoelectric effect goes back to 19th century. First demonstration of the piezoelectric effect by Currie brothers (Pierre and Jacques) was done in 1880. Since then, lots of work has been done on the development of various piezoelectric materials. The main breakthrough in the field came during early to mid 1940's, with the development of ABO_3 type perovskite structure.[3] Lead zirconate titanate $(1-x)PbZrO_3$ $xPbTiO_3$ (PZT) is the most important piezoelectric material which was developed in 1950's, and after 50 years it remains the most widely used piezoelectric ceramic.

Large piezoelectric coefficient, large coupling factor and high Curie temperature (T_C) makes this material suitable for a wide range of piezoelectric applications. PZT has $T_C \sim 386^0$C and shows rapid thermal degradation above 200^{0}C.[3] There are several applications where piezoelectric materials are required to operate above this temperature range.

The piezoelectric effect includes two types of responses; direct and converse. Production of electric charge when stress is applied is known as direct piezoelectric effect whereas the production of stress and/or strain when an electric field is applied is known as converse piezoelectric effect. Fig. 1 shows the schematic illustration for direct and converse piezoelectric effect

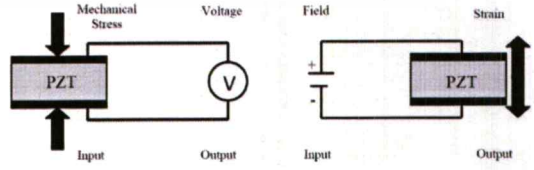

Figure 1 Schematic for a)direct and b)converse piezoelectric effects

The perovskite structure applies to series of compounds with three types of atoms with general formula ABO_3 described by a simple cubic unit cell with oxygen atoms at the face centers, larger cations at the cube corners (A sites) and smaller cations in body center(B sites). Typical perovskite ABO_3 unit cell is shown in Fig. 2. There are many complex perovskites which can be describe with the formula $(A',A'')^{XII}(B',\ B'')^{VI}O_3$, where XII and VI represent coordination numbers.

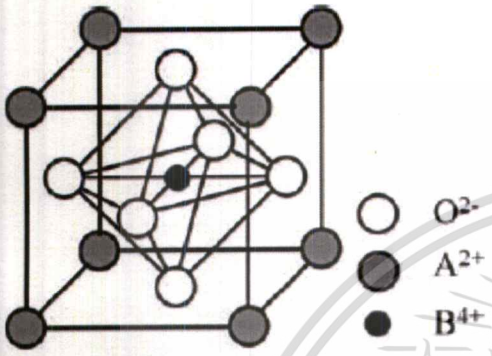

Figure 2 Perovskite Unit Cell ABO3 unit cell

In PZT, Pb^{2+} ions are situated at the corner of the unit cell (A sites), Zr^{4+} or Ti^{4+} at body center positions (B site). In BSPT, Pb^{2+} and Bi^{3+} share the A sites whereas Ti^{4+} and Sc^{3+} share the B sites. In both materials O^{2-} is situated at face center position forming octahedra around the B site (BO_6).

Ideal perovskite structure is simple cubic lattice. Depending on the ionic radii of cations and anions the perovskite unit cell may be distorted to rhombohedral or tetragonal symmetry Type of the perovskite crystal structure can be predicted using Goldschmidt tolerance factor (t), given in equation (1.1).[3]

$$t = (RA + RO) / \sqrt{2}\,(RB + RO) \quad (1.1)$$

where RA, RB, and RO are the ionic radius of large cation, small cation, and anion respectively. In general it is observed that perovskite structures with t = 0.95 – 1.0 are cubic, t < 0.95 - rhombohedral or monoclinic, and t > 1.0 - tetragonal. Polarization direction for rhombohedral is <111>, for tetragonal <001>, and for monoclinic phase it contained in monoclinic plane between [001] and [111].[4] This provide 8 equivalent polarization states for rhombohedral and 6 for tetragonal. In the case of a monoclinic ferroelectric phase the polarization may continuously rotate between up to 24 different states.

Ferroelectric materials posses a local spontaneous polarization and shows hysteresis relation between polarization and applied electric field. This behavior is observed in certain temperature region which depends on the transition of ferroelectric phase to paraelectric phase. Temperature above which the material loses its spontaneous polarization and piezoelectric characteristics is known as ferroelectric Curie temperature (Tc).

As the temperature is increased, near T_C the dipoles have the tendency to revert back to random orientation. Degradation of piezoelectric properties due to loss of polarization is called thermally activated aging. In order to minimize the aging effect, maximum applications of materials are restricted to ~½T_C.52 PZT has $T_C \sim 386^0$C and shows rapid degradation above 200^0C.[3]

As discussed in section 1.1, the piezoelectric effects include two types of responses; direct and converse. The basic mathematical equations (1.2) and (1.3) describe the above two types of piezoelectric effects are,

$$D = d\,.\,T \text{ (Direct piezoelectric effect) (1.2)}$$

$$S = d\,.\,E \text{ (Converse piezoelectric effect) (1.3)}$$

where D is the dielectric displacement, T the stress, S the mechanical strain, E the electric field, and d the piezoelectric constant which is numerically constant for both effects [3]

Piezoelectric properties are also anisotropic and vary with direction of polarization axis and strain, hence may be specified in tensor form as in equation (1.4) to indicate directionality.

$$D_i = d_{ijk}\,.T_{jk} \text{ and } S_{jk} = d_{ijk}\,.\,E_i \quad (1.4)$$

Depending on the application, piezoelectric devices may use one of the above piezoelectric effects. High d is desirable for actuator applications like ultrasonic cleaner transducers, where materials are intended to develop motion or vibrations.

Another frequently used piezoelectric constant is g*ij* which is related to d by equation (1.5).[3]

$$g = d / \varepsilon = d / K\varepsilon 0 \quad (1.5)$$

where ε the dielectric permittivity of material, and ε0 the dielectric permittivity of vacuum. High g is desirable for sensors applications like pressure sensors, where materials are intended to generate voltage in response to mechanical stress.

II. EXPERIMENTS

A. Apparatus

Scanning electron microscope (SEM) is one of failure analysis (FA) equipments that can visually inspection on all stroke failures head with very high magnification to verify any mechanical damage to the PZT bonded area.

X-Ray machine is another of FA equipments that can visually inspect the failed parts to verify any mechanical damage to the PZT bonded area.

Multi meter with nano probe to measure capacitance of the stroke failure parts and will use it for micro process mapping in HGA manufacturing process and characterize the PZT performance without performing flying head over the recording media at electrical tester.

Electrical tester is recording head computerized test system that can measure and characterize the stroke failure parts. It can vary bias voltage to the part and measure head

movement in each direction according to the bias voltage apply onto the parts.

Thermocouple and PICO gage are used to measure temperature at slider attach and infrared oven cure machine set up.

Figure 3. Thermocouple and PICO gage

B. Samples

The heads for this experiment are new suspension with piezoelectric on suspension near gimbal area.

C. Experimental Methods

To verify and characterize the stroke failure parts, X-Ray machine and SEM were used to verify any mechanical damage to the parts at PZT bonded area underneath the piezoelectric. In the mean time, we also performed HGA line mapping by using multi-meter to measure capacitance and resistance of piezoelectric to identify which station causing capacitance changed/degraded. Then, we optimized the station by using thermocouple with pico gage to measure temperature at each station that causing the capacitance changed/degraded.

III. RESULTS

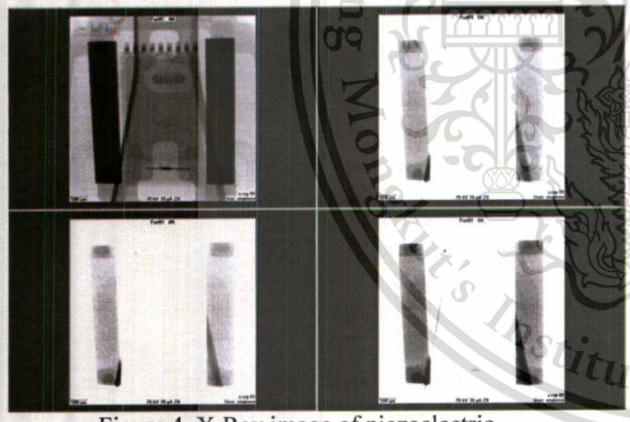

Figure 4. X-Ray image of piezoelectric

All Stroke failure parts have been verified for mechanical damage to the piezoelectric on suspension by X-Ray machine. The X-Ray images showed no mechanical damages found at all joint areas (Fig. 4).

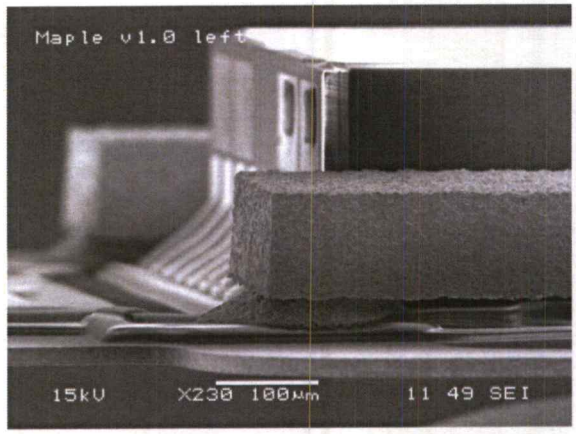

Figure 5. SEM image of at side of piezoelectric

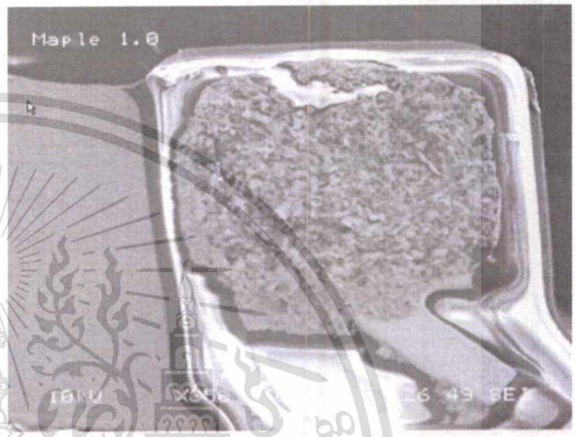

Figure 6. SEM image of bonded surface after shear Test

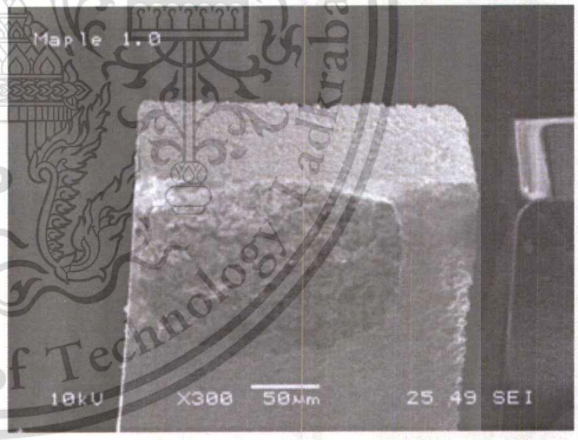

Figure 7. SEM image of bonded surface after shear Test

Fig. 5 shows SEM image with high magnification inspection on all stroke failure parts. There are no mechanical damage and also surface both side of piezoelectric are in good condition. Moreover after shear test at bonded area, there are no any abnormal structures found on both suspension joint and piezoelectric joint area. The adhesive joint area was in good shape in Figs. 6 and 7.

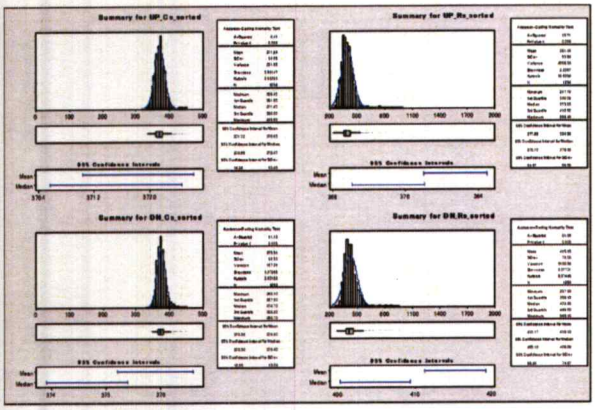

Figure 8 Capacitance and resistance measurement of piezoelectric at incoming parts (suspension level)

The capacitance and resistance measurement has been performed at incoming parts (Raw Suspension) by using multi meter and the result show both capacitance and resistance are acceptable on an average 370pF both tabs and 400Ω respectively as show in Fig. 8.

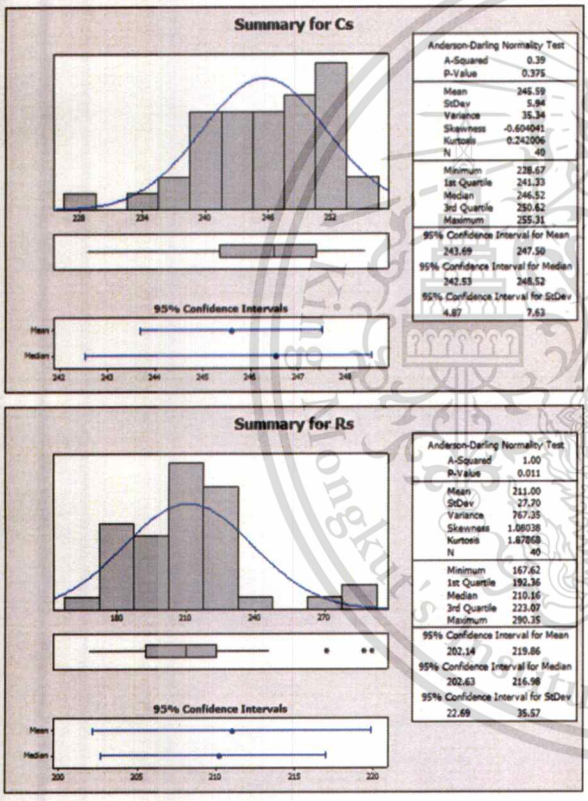

Figure 9. Capacitance and resistance measurement of piezoelectric for stroke failure parts

The capacitance and resistance measurement has been performed for all stroke failure parts from electrical tester by using multi meter and the results show both capacitance and resistance rejected with an average 245pF both tabs and 211Ω respectively as show in Fig. 9. It was confirmed for true failure.

No.	TGA Level	HGA Level	HGAs After ET
1	0.418	0.3	0.306
2	0.417	0.28	0.283
3	0.415	0.297	0.172
4	0.427	0.285	0.285
5	0.418	0.287	0.285
6	0.426	0.298	0.286
7	0.532	0.292	0.289
8	0.418	0.299	0.289
9	0.423	0.296	0.288
10	0.413	0.291	0.288
11	0.405	0.289	0.285
12	0.426	0.291	0.286
13	0.428	0.297	0.289
14	0.427	0.295	0.29
15	0.413	0.287	0.287
Average	0.427	0.292	0.281
		31%	34%

Table 1. Capacitance line mapping process by using multi meter

The capacitance line mapping has been performed by using multi meter in head gimbal assembly process and the results show no issues found at incoming suspension only in head gimbal assembly process at slider attach and infrared oven cure machine can cause the capacitance dropped in approximately 30% from incoming as show in Table 1.

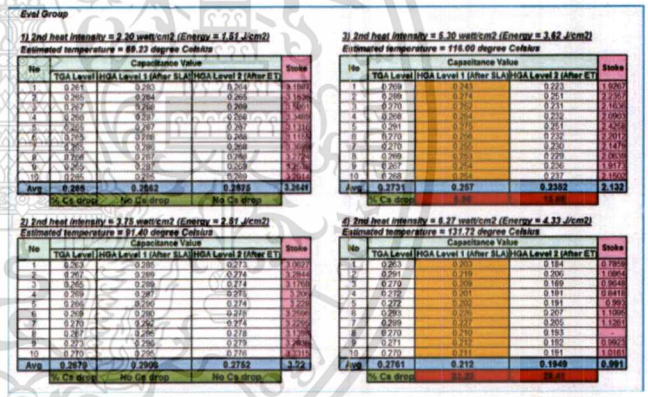

Temperature calcuated from regression equation below.

Temperature vs IR Energy regression
Temperature (oC) = 35.77 + 22.16 IR Energy(J/Cm2)

(1.6)

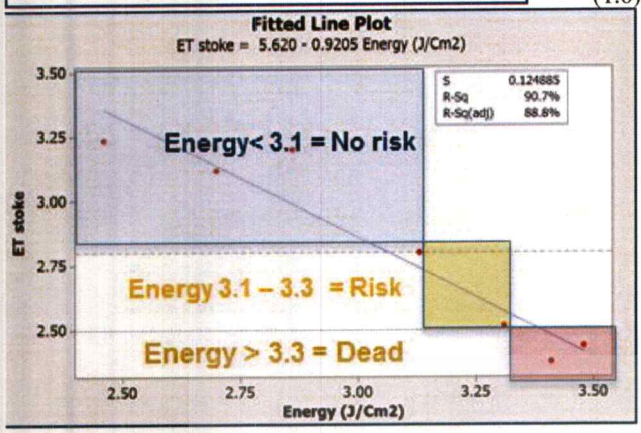

Figure 10. Infrared energy level optimization

The Infrared energy level has been studied and optimized to be able to control heat transfer to the piezoelectric on suspension by using temperature regression equation(1.6) above and also in Fig. 10. The safe zone for energy must be less than 3.1 J/cm^2

	Stroke Failure			After re-poling PZT		
	Left PZT	Right PZT	Both PZT	Left PZT	Right PZT	Both PZT
Part 1	120.9	120.9	246	158.9	163.7	377
Part 2	132	118.3	247	154.1	164.3	379
Part 3	133.3	116.1	251	149.7	158.6	380
Part 4	132.4	112.1	252	160	154.7	381

Table 2. Capacitance measurement after re-poling PZT

	Stroke Failure (nm/V)	After re-poling PZT (nm/V)
Part 1	-95.72	-86.55
Part 2	-77.35	-85.53
Part 3	-88.56	-86.33
Part 4	-91.03	-86.41
Part 5	-94.58	-86.48

Table 3. Mechanical normalized stroke measurement after re-poling PZT by using Wave C

From an infrared energy experimental result, it has been indicated that the cause of piezoelectric has been degraded at slider attach and infrared oven machine from heat transfer which is more than half of curie's temperature of piezoelectric material. The Stroke failures have been confirmed by re-poling the piezoelectric and measure capacitance and stroke. The result shows after re-poling piezoelectric the capacitance and the normalized stroke reading are back to normal with acceptable in an operating range.

IV. CONCLUSIONS

The experiment results show no mechanical damage related issue by using X-Ray and SEM inspection technique. Also an incoming suspension has no issue. The capacitance line mapping shows Slider attach and Infrared Oven Cure machines are cause of problem. The Infrared energy optimization has been studied and showed with energy higher than 3.1 J/cm^2 can cause piezoelectric on suspension degraded or dead from heat transfer per temperature regression equation. Once the temperature increases over half of curie's temperature, piezoelectric material starts to degrade.

ACKNOWLEDGMENT

First of all, I would like to thank you Dr. Winadda and Assoc. Prof. Dr. Wanchai , my Advisor and Co-Advisor respectively for their very helpful recommendation and suggestions with a constant supports of my research at KMITL. I am also thank you to all Thesis committee members for their constructive comments and helpful discussion which guide me a better understanding and perspective on my own result. I also should mention that my graduate study in King Monkut's Instisute of Technology Ladkrabang was supported by NSTDA, KMITL and Seagate Technology (Thailand) Ltd.

And finally, I would like to acknowledge the support of my family and f riends for all of their help.

REFERENCES

[1] A. Barzegar, R. Bagheri and A.K. Taheri, "Aging of piezoelectric composite transducers," *Journal of Applied Physics*, **89**

[2] B. Guiffard, E. Boucher, L. Lebrun, and D. Guyomar, Characteristics of F doped PZT ceramics using different fluorine sources," *Material Science and Engineering*, **137**, (2007)

[3] B.Jaffe, W.R. Cook, and H. Jaffe, *Piezoelectric ceramics* (Academic Press, New York, 1971)

[4] B. Noheda, "Structure and high piezoelectricity in lead oxide solutions,"*Current Opinion in Solid State and Material*, **6**, (2002)

[5] D.Damjanovic, and M. Demartin, "Contribution of the irreversible displacement of domain walls to the piezoelectric effect in barium titanate and lead zirconate titanate ceramics," *Journal of Physics: Condens Matter*, **9**, (1997)

[6] G.H. Haertling, "Ferroelectric ceramics: History and technology," *Journal of American Ceramic Society*, **82**, (1992)

BIOGRAPHY

Name: Mr. Hussadin Thungsakul

Date of Birth: October 19,1967

Place of Birth: Nakhorn Phanom, Thailand

Educations:

1989 King-Mongkut Institute of Technology North-Bangkok, Faculty of Engineering

Scholarships:

2009-2010 Scholarship for study in the M. Eng. Of Data Storage Technology (English Program) by NSTDA, KMITL and Seagate Technology (Thailand) Ltd.

Publications:

1. Hussadin Thungsakul, Wanchai Pijitrojana and Winadda Wongwiriyapan "Suspension with Piezoelectric Effects on High Temperature in HGA Manufacturing Process" 2013